

Modeling Pc4 Pulsations in Two and a Half Dimensions

DRAFT VERSION CREATED ON FEBRUARY 12, 2016

© Charles A McEachern 2016
ALL RIGHTS RESERVED

Acknowledgements

Acknowledgement placeholder.

Dedication

Dedication placeholder.

Abstract

Something something Pc4 pulsations. Ultra low frequency (ULF) waves with periods of a minute or two. They correspond to field line resonances near Earth's plasmapause. Drift or drift-bounce resonance with energetic radiation belt and ring current particles. Radial diffusion.

Pc4 pulsations are known to exhibit different behavior based on their azimuthal mode-number. Low- m Pc4 pulsations are driven at the outer edge of the magnetosphere, and have a compressional component. High- m Pc4 pulsations are non-compressional and are driven within the magnetosphere.

Giant pulsations are a subset of high- m Pc4 pulsations which are of particular interest. High- m Pc4 pulsations are hard to simulate. Traditionally, simulations are driven from the outer boundary, which doesn't work in this case. And resolving high azimuthal modenumbers is computationally expensive in a 3D simulation.

Chapter 1 gives a general introduction is made to Earth's magnetosphere. (Note: this doesn't exist yet.)

Chapter 2 summarizes Pc4 pulsations in terms of prominent theoretical and observational work, including work on giant pulsations. (Note: this mostly doesn't exist yet.)

Chapter 3 presents a 2.5D model designed to simulate Pc4 pulsations, including those with high azimuthal modenumbers. The model is built upon recent work by Lysak, and includes a dipole-aligned geometry, a height-resolved ionosphere, and coupling to a conducting Earth. Ring current modulation is introduced as a novel driving mechanism.

Chapter 4 derives dispersion relations for a cold, resistive plasma, such as Earth's inner magnetosphere and ionosphere. This gives an idea as to the waves expected to be produced.

Chapter 6 compares model output to poloidal Pc4 observations made with the Van Allen Probes. (Note: this hasn't quite happened yet. The chapter briefly explains.)

Chapter 5 investigates the results of adding electron inertial effects to the model, allowing the computation of parallel electric fields and field-aligned currents.

Chapter 7 showcases changes in Pc4 behavior as a result of altering the azimuthal modenumber. This includes a rotation of poloidal to toroidal waves, significantly refining past work by Mann, and before that Radoski. (There are a lot of figures here. It might end up being two chapters.)

Chapter 8 offers a summary and possibilities for future work.

NOTE: ALL FIGURES ARE PDFS. Some of the frames are small, but they should remain sharp when you zoom in on them.

Contents

Acknowledgements	i
Dedication	ii
Abstract	iii
List of Tables	viii
List of Figures	ix
1 The Near-Earth Environment	1
1.1 The Outer Magnetosphere	1
1.1.1 The Magnetopause	2
1.1.2 The Magnetotail	2
1.1.3 Cusp Regions	2
1.2 The Inner Magnetosphere	2
1.2.1 The Plasmasphere	2
1.2.2 Ring Currents	2
1.2.3 The Radiation Belts	2
1.3 The Ionosphere	2
1.3.1 Field-Aligned Currents	3
1.3.2 Pedersen and Hall Currents	3
1.3.3 Ionospheric Stratification	3
1.4 Geomagnetic Disturbances	3
1.4.1 Storms	3

1.4.2	Substorms	3
2	Magnetic Pulsations	4
3	Numerical Model	6
3.1	Coordinate System	8
3.1.1	Covariant and Contravariant Bases	10
3.1.2	Mapping to Physical Coordinates	11
3.2	Ionospheric Profile	12
3.2.1	Conductivity	12
3.2.2	Alfvén Speed	13
3.3	Maxwell's Equations	17
3.3.1	Notation and Optimization	17
3.3.2	Magnetic Fields	18
3.3.3	Electric Fields	18
3.4	Driving	21
3.4.1	Outer Boundary Compression	21
3.4.2	Ring Current Modulation	24
3.5	Boundary Conditions	26
3.5.1	Parity and Interpolation	26
3.5.2	Coupling to the Atmosphere	27
4	Waves in Cold Resistive Plasmas	31
4.1	Parallel Propagation Limit	33
4.1.1	Parallel Polarization	33
4.1.2	Perpendicular Polarization	34
4.2	Perpendicular Propagation Limit	34
4.2.1	Parallel Polarization	35
4.2.2	Perpendicular Polarization	35
4.3	High Altitude Limit	36
4.3.1	Azimuthal Polarization	36
4.3.2	Meridional Polarization	36
4.4	Implications for This Work	37

4.4.1	Mode Coupling	37
4.4.2	High Modenumber Cutoff	37
5	Electron Inertial Effects	38
5.1	The Boris Approximation	39
5.2	Effect on the Simulation	41
5.3	Field-Aligned Current	42
5.4	Inertial Length Scales	44
6	Comparison to Van Allen Probes	46
7	Large Modenumber Effects	47
7.1	Finite Poloidal Lifetimes	47
7.2	Resonant Shells	50
7.3	Significance for Giant Pulsations	56
7.4	Electromagnetic Energy Gap	57
8	Conclusion	60
8.1	Summary of Results	60
8.2	Future Work	60
References		61
Appendix A. Differential Geometry		65
A.1	Glossary	65
A.2	Acronyms	65

List of Tables

A.1 Acronyms	65
------------------------	----

List of Figures

3.1	Nonorthogonal Dipole Grid	10
3.2	Ionospheric Conductivity Profiles	13
3.3	Alfvén Speed Profiles	15
3.4	Alfvén Bounce Frequency Profiles	16
3.5	Decreasing Penetration with Increasing Modenumber	23
3.6	Sym-H Fourier Components for June 2013 Storm	25
5.1	Magnetic Field Comparison With and Without Electron Inertial Effects	41
5.2	Field-Aligned Current and Poynting Flux at the Ionosphere	43
5.3	Ionospheric Power Density	44
7.1	Current-Driven Poloidal and Toroidal Energy: 22mHz	49
7.2	Poloidal Energy Density by L-Shell: 22mHz	52
7.3	Poloidal Energy Density by L-Shell: 10mHz	53
7.4	Toroidal Energy Density by L-Shell: 22mHz	54
7.5	Toroidal Energy Density by L-Shell: 10mHz	55
7.6	Current-Driven Electric and Magnetic Energy: 10mHz	58
7.7	Current-Driven Electric and Magnetic Energy: 22mHz	59

Chapter 1

The Near-Earth Environment

TODO: So far, this chapter is just a tentative outline.

It's all about energy transfer! Sun generates energy through nuclear reactions. Some of this energy is transported in the solar wind, which drives behavior in the near-Earth environment.

At Earth's orbit, the solar magnetic field makes more-or-less a 45° angle with the X axis.¹

1.1 The Outer Magnetosphere

The outer magnetosphere is a region where the field lines are closed, but significantly deformed by the solar wind.

¹Uppercase X , Y , and Z are used to indicate GSE coordinates: X points from the Earth to the Sun; Y is perpendicular to X in the Sun's ecliptic plane, pointing duskwards; Z points north, out of the ecliptic plane. In later chapters, lowercase x , y , and z are used to define a more-or-less analogous coordinate system with respect to Earth.

1.1.1 The Magnetopause

1.1.2 The Magnetotail

1.1.3 Cusp Regions

TODO: The cusp regions might not even need to be mentioned... they're not specifically important here.

1.2 The Inner Magnetosphere

In the inner magnetosphere, field lines are closed, and are approximately dipolar.

1.2.1 The Plasmasphere

1.2.2 Ring Currents

1.2.3 The Radiation Belts

1.3 The Ionosphere

The ionosphere is immediately above Earth's neutral atmosphere.

1.3.1 Field-Aligned Currents

1.3.2 Pedersen and Hall Currents

1.3.3 Ionospheric Stratification

1.4 Geomagnetic Disturbances

1.4.1 Storms

1.4.2 Substorms

Chapter 2

Magnetic Pulsations

TODO: This chapter will lay out the basics of ULF waves, specifically Pc4 pulsations and giant pulsations. Notable steps in theory and observation will be summarized. For now, it's mostly a disorganized mishmash of citations.

"To summarize, the general buffetting of the magnetosphere by variations in the solar wind dynamic pressure, or perhaps by sporadic magnetic reconnection, provides a broad band energy source to the magnetosphere. The magnetospheric cavity as a whole rings at its own eigenfrequencies, thus transporting energy at just those frequencies to field lines deep in the magnetosphere. Those field lines whose eigenfrequencies match one of the cavity eigenfrequencies couple to the cavity mode and resonate strongly, producing the classical field line resonance signature.[1]"

Dungey's Alfvén wave paper[2].

High-modenumber ULF pulsations are damped by the ionosphere, making it more difficult to observe them on the ground[3]. Small structures are also damped; resonances narrower than ~ 100 km aren't visible on the ground.

TODO: See also Glassmeier and Stellmacher, 2000 (about small latitude), and Wright and Yeoman, 1999, Yeoman and Wright, 2001 about large m

Multi-spacecraft observation of a ULF wave with very high modenumber (70+) and no apparent ground signature[4].

A recent survey of Van Allen Probe data showed that Pc4 pulsations – the poloidal ones, at least – occur primarily during geomagnetically active times, near the plasmapause, over just a handful of hours of dayside MLT[5]. This confirmed and refined older work[6].

ULF waves have been shown to correlate with pulsating aurora and with chorus[7]. It's believed that (in the case presented) substorm injection drove Pc4-5 pulsations, which modulated chorus waves, which pitch-angle scattered electrons with energies on the order of 10 keV.

Energetic ring current and radiation belt particles can be accelerated by ULF waves through drift or drift-bounce resonance[8].

A Hall-conducting ionosphere reflects ULF waves[9].

"It is not clear why noncompressional [high- m] Pc4 poloidal waves, which are presumably driven by instability within the magnetosphere, preferentially occur on the dayside.[5]"

Poloidal and toroidal ULF polarizations are treated differently by the ionosphere[10] (or, more recently, [11]).

TODO: Theoretical consideration of decay vs propagation, by frequency. Lysak and Yoshikawa 2006.

TODO: Fishbone instability. McGuire 1983, Chen 1984. Similar phenomenon, but for lab plasmas.

An ideal poloidal mode decays to the toroidal mode in the presence of curved magnetic field lines[12] or a gradient in the Alfvén speed[13]. The time is proportional to the azimuthal wavenumber[13]. An analytical follow-up agreed with the numerical work[14].

TODO: Mann gives the poloidal-to-toroidal decay time to be $\tau = \frac{d\lambda}{d\omega'_A}$, where $\lambda = \frac{m}{2\pi r}$ and ω'_A is the spatial derivative of the Alfvén bounce frequency, but this doesn't seem to line up. When τ is computed using our Alfvén bounce frequencies, the result is much less than 1 s. Double-checking is necessary.

Chapter 3

Numerical Model

The model works in two and a half dimensions. A meridional slice of the magnetosphere is resolved. Fields are presumed to vary azimuthally according to a fixed modenumber m . Derivatives in ϕ are replaced by im . Imaginary field values indicate a phase shift in the azimuthal direction.

TODO: From Bob's 2013 paper[15] (which was also 2.5D): "The shear Alfvén and compressional fast mode waves can be coupled not only by the Hall conductivity but also by inhomogeneities in the background plasma, which are unavoidable in a realistic magnetosphere [e.g., Lysak and Yoshikawa, 2006[16]; Waters et al., 2012[17]]. This coupling requires a finite wave vector component in the azimuthal direction, i.e., a finite m in the context of the present model. Because of the $\exp(im\phi)$ dependence assumed in this model, the coupling from the inhomogeneity enters as an imaginary part of the coupled wave fields with respect to the initial fields, whereas the Hall conductivity appears in phase with the initial fields. Thus, although a fully three-dimensional model can give a more complete picture of wave propagation [e.g., Lysak, 2004[18]; Woodroffe and Lysak, 2012[19]], the present two-dimensional model serves to illustrate the nature of this coupling."

The use of a fixed modenumber allows a dramatic decrease in computational cost. Waves with very high azimuthal modenumber are prohibitively expensive to simulate since they can only be resolved if grid resolution is very fine in the azimuthal direction.

TODO: Can we find a citation where someone explicitly talks about the computational cost of high- m simulations? Or is it just obvious Nyquist?

This prevents the simultaneous consideration of dayside and nightside phenomena, but is fine for azimuthally-localized waves. As was shown by [6], and recently confirmed in detail by [5], Pc4 pulsations are generally confined to just a few hours MLT on the dayside.

Driving with a compressional pulse from the outer boundary of a simulation is typical. This model also includes a novel driving mechanism: perturbations to the ring current.

The code is linear. All magnetic fields are a first-order perturbation over the zeroth-order dipole field. This is a not-great assumption out towards the magnetopause. In practice, however, most activity is within $L \sim 7 R_E$, where the dipole approximation is pretty good.

Models with height-resolved ionospheres are a very recent development. Lysak presented his in 2013[15].

Ground signatures are fairly recent as well.

TODO: Some ground signature work as far back as Greifinger and Greifinger in 1968[10], but there's been steady advancement. Lysak and Song, in 2006, were the first to work out ground signatures without the assumption of a single-frequency wave.

TODO: The support software – the driver and the plotter – are significant too. Do they go in a section? In an appendix?

TODO: Past FLR simulations focused on a single mode, didn't account well for the ionosphere, etc. Lee and Lysak 1989, 1990, 1991, Rankin et al 1993, 1995, 1999, Tikhonchuk and Rankin 2000, 2002.

TODO: Past work that got ground signatures (without latitude-dependent zenith angle) Greifinger and Greifinger 1968, 1973, Hughes 1974, Sciffer and Waters 2002, Sciffer et al 2005. Better computation of ground signatures... Waters and Sciffer 2008, Sciffer and Waters 2011, Woodroffe and Lysak 2012.

Note that the model uses megameters, seconds, megacoulombs, and grams as the fundamental units of length, time, charge, and mass respectively. As a result, electric field is measured in mV/m, magnetic field is measured in nT, and Poynting flux is measured in mW/m². The electric constant is expressed in mF/m, not in units of ϵ_0 , not that it really matters.

3.1 Coordinate System

When referring to fields in place, it's convenient to use lowercase¹ x , y , and z in their usual dipolar sense. The unit vector \hat{z} is aligned with the dipole field (pointing outward in the northern hemisphere and inward in the southern hemisphere), while \hat{x} is perpendicular to \hat{z} within the meridional plane and \hat{y} points in the azimuthal direction.

TODO: Double-check the signs for x (radially inward or outward at the equator?) and y (east or west?).

TODO: Wait... are x , y , and z the same as Radoski's coordinates?

It's convenient to align the grid with the zeroth-order magnetic field, which is presumed to be a perfect dipole. Field line resonances (such as Pc4 pulsations) are guided by magnetic field lines.

TODO: “ULF waves can be guided.” Cite.

A typical outermost field line has an equatorial radius of $10 R_E$. At this point, the ideal dipole approximation is suspect, particularly on the dayside. In practice, however, most wave activity is concentrated around $L \sim 7$.

Radoski did theoretical work in the following dipole coordinates[20].

$$\mu = -\frac{\sin^2 \theta}{r} \quad \phi = \phi \quad \nu = \frac{\cos \theta}{r^2} \quad (3.1)$$

TODO: The symbol ν is overused. Reserve it for collision frequency. Use something else here.

¹Not to be confused with uppercase X , Y , and Z , which orient relative to the sun; see Chapter 1

It's also convenient to take into account the effects of the ionosphere, the lower boundary of which is governed by gravity, and thus has a more-or-less constant altitude. If the above coordinates are used, no line of constant ν coincides with the ionosphere, at least not over a significant range of latitudes.

Many previous works have used an effective ionosphere of nonuniform altitude.

TODO: Figure out which previous works are worth citing here. Options include Radoski 1967, Lee and Lysak 1989, 1991, Rankin et al 1993, 1994, Streltsov and Lotko 1995, 1999.

TODO: “The ionosphere is important for Alfvén waves” Cite?

In order to accommodate dipole field lines as well as a fixed-altitude ionosphere, a nonorthogonal grid is necessary. Such a grid was worked out numerically by Proehl[21], then formalized analytically by Lysak[18]:

$$u^1 = -\frac{R_I}{r} \sin^2 \theta \quad u^2 = \phi \quad u^3 = \frac{R_I^2}{r^2} \frac{\cos \theta}{\cos \theta_0} \quad (3.2)$$

The term R_I indicates the ionosphere's position relative to Earth's center. It's generally taken to be $1 R_E + 100 \text{ km}$.

Like μ and ϕ , the coordinates u^1 and u^2 index a field line. However, compared to ν , u^3 has been renormalized by $\cos \theta_0$, where θ_0 is the colatitude where each field line intersects the ionosphere in the northern hemisphere. As a result, for all field lines, $u^3 = \pm 1$ at the northern and southern foot points.

In terms of the McIlwain parameter, $u^1 = -\frac{R_I}{L}$, and $\cos \theta_0 = \sqrt{1 - \frac{R_I}{L}}$

Compared to Equation (3.1), Equation (3.2) represents a renormalization of indexing along each field line. The field lines themselves are not deformed.

TODO: Explain how we set up the grid. It should only take a paragraph or two – it doesn't need its own section.

Nonorthogonal Dipole Grid

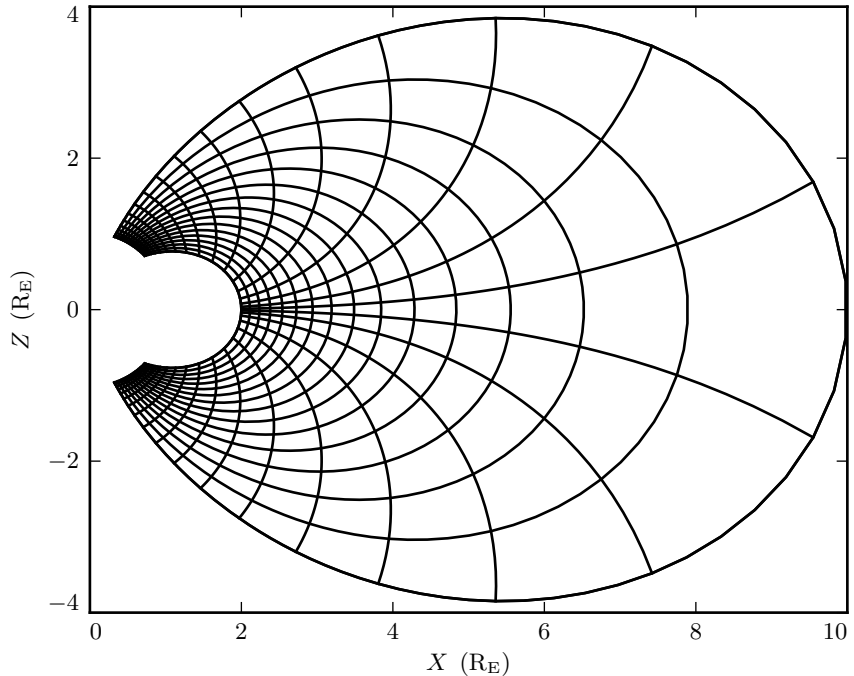


Figure 3.1: The model’s nonorthogonal dipole grid. Only every fifth point is shown in each direction. The grid resolution is highest near the ionosphere and lowest at large distances. The high concentration of grid points at the inner edge of the equator is a consequence of renormalizing the grid spacing with $\cos \theta_0$; whereas Radoski’s dipole coordinates come to a singularity at the center of the Earth, Lysak’s coordinates converge at the equatorial ionosphere.

3.1.1 Covariant and Contravariant Bases

The coordinates defined in Equation (3.2) are not orthonormal. As a result, it’s necessary to consider covariant and contravariant basis vectors separately.

Covariant basis vectors $\hat{e}_i \equiv \frac{\partial}{\partial u^i} x$ are normal to the curve defined by constant u^i .

Contravariant basis vectors $\hat{e}^i \equiv \frac{\partial}{\partial \underline{x}} u^i$ are tangent to the coordinate curve. Equally, they're normal to the plane defined by constant u^j for all $j \neq i$.

The basis vectors are reciprocal to one another[22], and can be used to define the metric tensor g .

$$\hat{e}^i \cdot \hat{e}_j = \delta_j^i \quad \hat{e}_i \cdot \hat{e}_j = g_{ij} \quad \hat{e}^i \cdot \hat{e}^j = g^{ij} \quad (3.3)$$

Note δ_j^i is the Kronecker delta, ε^{ijk} is the Levi-Civita symbol, and summation is implied over repeated indeces per Einstein's convention[23].

The metric tensor is used to map between the covariant and contravariant representations of a vector

$$A_i = g_{ij} A^j \quad \text{and} \quad A^i = g^{ij} A_j \quad \text{where} \quad A_i \equiv \underline{A} \cdot \hat{e}_i \quad \text{and} \quad A^i \equiv \underline{A} \cdot \hat{e}^i \quad (3.4)$$

The Jacobian, used for mapping differential volume elements between bases, can be expressed as the square root of the determinant of the metric tensor.

$$G du^1 du^2 du^3 = dV \quad \text{where} \quad G = \sqrt{\varepsilon^{ijk} g_{1i} g_{2j} g_{3k}} \quad (3.5)$$

This quantity is also used when expressing a curl or cross product in generalized coordinates.

$$(\nabla \times \underline{A})^i = \frac{\varepsilon^{ijk}}{G} \frac{\partial}{\partial u^j} A_k \quad (\underline{A} \times \underline{B})^i = \frac{\varepsilon^{ijk}}{G} A_j B_k \quad (3.6)$$

3.1.2 Mapping to Physical Coordinates

The full expression for the basis vectors, metric tensor, and Jacobian determinant discussed in Section 3.1.1 can be found in the appendix of [18].

TODO: These expressions should probably be written out an in appendix here too...

The basis vectors can be renormalized to produce unit vectors along the dipole coordinates x , y , and z .

$$\hat{x} = \frac{1}{\sqrt{g^{11}}} \hat{e}^1 \quad \hat{y} = \frac{1}{\sqrt{g^{22}}} \hat{e}^2 \quad \hat{z} = \frac{1}{\sqrt{g^{33}}} \hat{e}^3 \quad (3.7)$$

In addition, this coordinate system provides horizontal and radial unit vectors. Note that Equation (3.8) is valid only at the ionospheric boundary.

$$\hat{\theta} = \frac{1}{\sqrt{g_{11}}} \hat{e}_1 \quad \hat{\phi} = \frac{1}{\sqrt{g_{22}}} \hat{e}_2 \quad \hat{r} = \frac{1}{\sqrt{g_{33}}} \hat{e}^3 \quad (3.8)$$

3.2 Ionospheric Profile

The ionospheric profiles used in this model are based on values tabulated in the Appendix B of Kelley's book[24]. They were adapted by Lysak[15] to take into account the effect of the magnetosphere's latitude-dependent density profile.

Mean molecular mass of 28 u at 100 km, 16 u around 400 km, down to 1 u above 1400 km.

Simulations are carried out using four profiles: active day, quiet day, active night, quiet night.

Profiles are static for the duration of a simulation. Even so-called ultra low frequency waves are still much faster than convective timescales.

TODO: Come up with a characteristic convective timescale or two, and cite it.

3.2.1 Conductivity

The effects of mean molecular mass on conductivity are computed per the usual definitions.

$$\sigma_P = \sum_s \frac{n_s q_s^2}{m_s} \frac{\nu_s}{\nu_s^2 + \Omega_s^2} \quad \sigma_H = - \sum_s \frac{n_s q_s^2}{m_s} \frac{\Omega_s}{\nu_s^2 + \Omega_s^2} \quad \sigma_0 = \sum_s \frac{n_s q_s^2}{m_s \nu_s} \quad (3.9)$$

Each profile is resolved to an altitude of about 10^4 km, and include well-resolved E , F_1 , and F_2 layers.

TODO: Talk about the ionospheric layers, probably in the introduction.

Pedersen (Blue), Hall (Red), and Parallel (Green) Conductivities

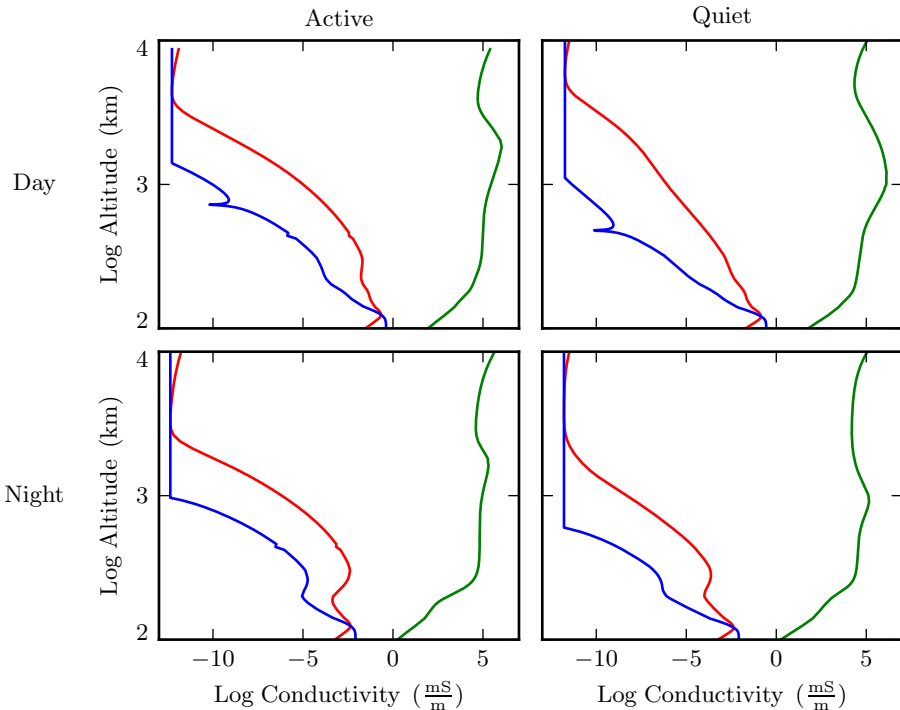


Figure 3.2: Ionospheric conductivity profiles, adapted by Lysak[15] from Appendix B of Kelley's textbook[24].

TODO: What is the height-interated conductivity for each profile?

3.2.2 Alfvén Speed

The Alfvén speed is computed from Kelley's low-density profile, modified to take into account the local density. The density, in turn, is the sum of a plasmaspheric profile

and a high-latitude auroral profile.

$$\epsilon_{\perp} = (\text{low-density tabulated value}) + \frac{n\bar{m}}{B_0^2} \quad (3.10)$$

TODO: What's a clean way of showing the low-density ϵ_{\perp} that we read in?

TODO: Does Kelley list the electric constant or the Alfvén speed?

Where \bar{m} is the ambient mean molecular mass and B_0 is the zeroth-order magnetic field strength, $B_0 = 3.11 \times 10^4 \text{ nT} \left(\frac{R_E}{r}\right)^3 \sqrt{1 + 3 \cos^2 \theta}$. Note that $3.11 \times 10^4 \text{ nT}$ is the value of the Earth's magnetic field at the equator on Earth's surface.

TODO: Cite this number?

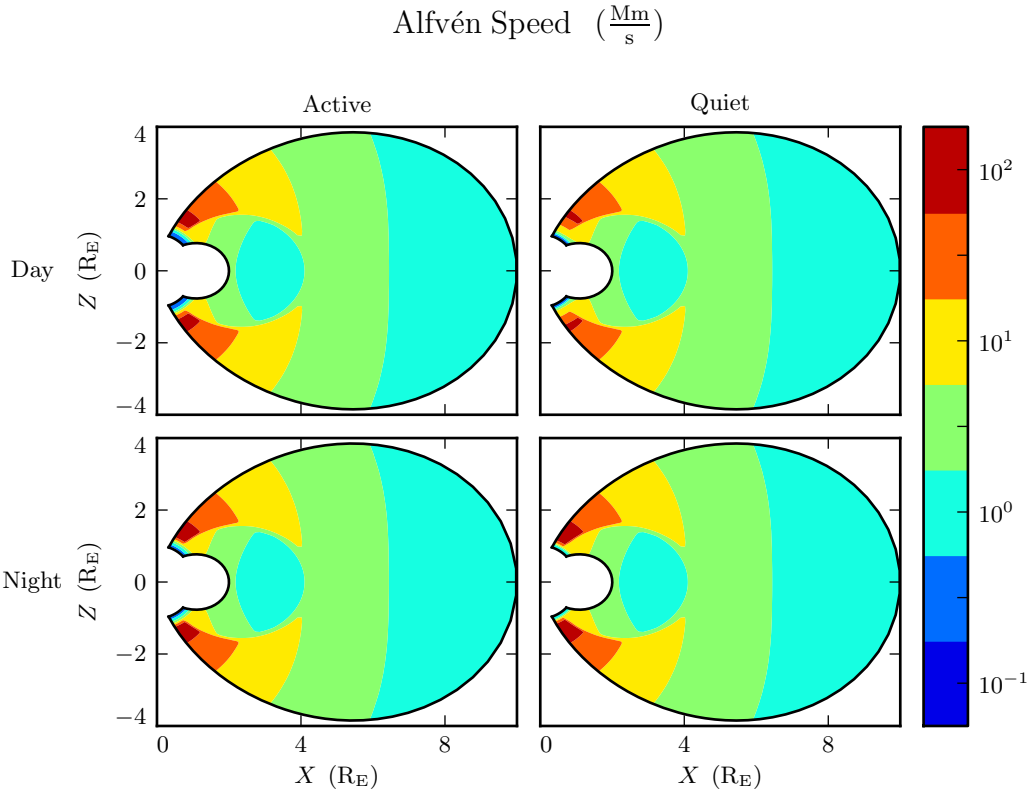


Figure 3.3: Alfvén speed profiles, adapted by Lysak[15] from Appendix B of Kelley's textbook[24].

TODO: Above the profile, Bob scales the value that's read in as r^5 or something. Is there a citation for that?

The Alfvén speed is then computed per $v_A^2 \equiv \frac{1}{\mu_0 \epsilon_{\perp}}$.

Alfvén Bounce Frequencies

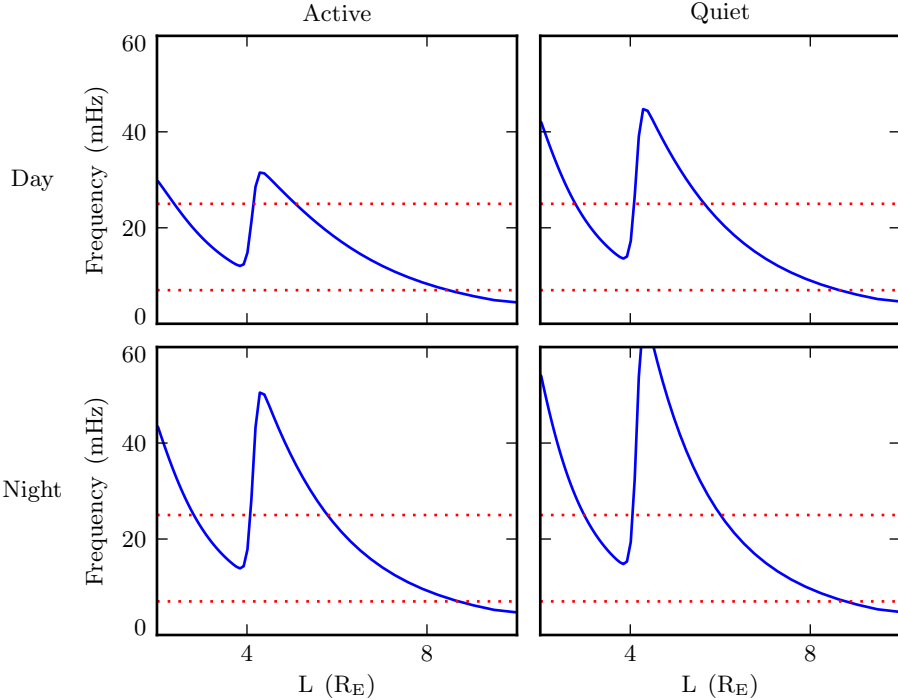


Figure 3.4: Alfvén bounce frequency profiles, computed by integrating the the Alfvén speed back and forth over a field line. $f_A = \left[\oint \frac{dz}{v_A} \right]^{-1}$. Dotted lines indicate the Pc4 frequency range, 7 mHz to 25 mHz. In each profile, the effect of the plasmapause is clearly visible, centered at $L = 4$. Field lines just inside and just outside the plasmapause appear susceptible to resonance in the Pc4 band.

TODO: Talk about how the size of the plasmasphere can be adjusted, and $4 R_E$ is just a typical value.

TODO: Explain how the Alfvén speed constrains the time step.

3.3 Maxwell's Equations

The model simulates the evolution of electric and magnetic fields in accordance with Maxwell's equations. Specifically, magnetic fields are advanced using Faraday's Law, and electric fields with Ampère's Law. Kirchhoff's formulation of Ohm's Law ($\underline{J} = \underline{\sigma} \cdot \underline{E}$) is used to eliminate the explicit current dependence in Ampère's Law.

$$\frac{\partial}{\partial t} \underline{B} = -\nabla \times \underline{E} \quad \underline{\epsilon} \cdot \frac{\partial}{\partial t} \underline{E} = \frac{1}{\mu_0} \nabla \times \underline{B} - \underline{\sigma} \cdot \underline{E} \quad (3.11)$$

3.3.1 Notation and Optimization

Algebra is carried out on paper, producing expressions where each field value is a linear combination of previous field values. These coefficients are computed before the main loop begins. This offers a significant reduction in floating point operations each iteration.

The \leftarrow operator is used to indicate assignment, rather than equality. Values on the left are new, and those on the right are old. New and old magnetic field values are offset by δt ; electric field values staggered by $\frac{\delta t}{2}$. As an example of this notation, Equation (3.12) integrates Faraday's Law over a time step, assuming that the curl of the electric field varies slowly compared to δt :

$$\begin{aligned} \int_0^{\delta t} dt \frac{\partial}{\partial t} \underline{B} &= - \int_0^{\delta t} dt \nabla \times \underline{E} \\ \underline{B}|_{\delta t} - \underline{B}|_0 &= -\delta t \nabla \times \underline{E}|_{\frac{\delta t}{2}} \\ \underline{B} &\leftarrow \underline{B} - \delta t \nabla \times \underline{E} \end{aligned} \quad (3.12)$$

It's also beneficial to store the curl of each field, rather than take derivatives on the fly. The following sections make use of the shorthand $\underline{C} \equiv \nabla \times \underline{E}$ and $\underline{F} \equiv \nabla \times \underline{B}$. Or, recalling Equation (3.6),

$$C^i = \frac{\varepsilon^{ijk}}{G} \frac{\partial}{\partial u^j} E_k \quad F^i = \frac{\varepsilon^{ijk}}{G} \frac{\partial}{\partial u^j} B_k \quad (3.13)$$

Only covariant field components are stored. Only contravariant curl components are

stored. This cuts down on memory use, while also eliminating the time spent rotating between bases; rotations between covariant and contravariant bases are built into the precomputed coefficients.

3.3.2 Magnetic Fields

Taking advantage of the shorthand defined in Equation (3.13), Faraday's Law is simply written

$$\frac{\partial}{\partial t} B^i = -C^i \quad (3.14)$$

Or, using the metric tensor to cast the magnetic field in terms of its covariant components, and writing out each coefficient explicitly,

$$\begin{aligned} B_1 &\leftarrow B_1 - g_{11} \delta t C^1 - g_{13} \delta t C^3 \\ B_2 &\leftarrow B_2 - g_{22} \delta t C^2 \\ B_3 &\leftarrow B_3 - g_{31} \delta t C^1 - g_{33} \delta t C^3 \end{aligned} \quad (3.15)$$

3.3.3 Electric Fields

Ampère's Law, can be solved with integrating factors. From Equation (3.11),

$$\underline{\epsilon} \cdot \frac{\partial}{\partial t} \underline{E} = \frac{1}{\mu_0} \nabla \times \underline{B} - \underline{\sigma} \cdot \underline{E} \quad (3.16)$$

The permittivity tensor can be trivially inverted.

$$\left(\underline{\Omega} + \underline{\underline{\epsilon}} \frac{\partial}{\partial t} \right) \cdot \underline{E} = \underline{\underline{v}}^2 \cdot \underline{F} \quad (3.17)$$

Where $\underline{\underline{\mathbb{I}}}$ is the identity tensor and in x - y - z coordinates,

$$\underline{\underline{v}^2} \equiv \frac{1}{\mu_0} \underline{\underline{\epsilon}}^{-1} = \begin{bmatrix} v_A^2 & 0 & 0 \\ 0 & v_A^2 & 0 \\ 0 & 0 & c^2 \end{bmatrix} \quad \text{and} \quad \underline{\underline{\Omega}} \equiv \underline{\underline{\epsilon}}^{-1} \cdot \underline{\underline{\sigma}} = \begin{bmatrix} \frac{\sigma_P}{\epsilon_{\perp}} & -\frac{\sigma_H}{\epsilon_{\perp}} & 0 \\ \frac{\sigma_H}{\epsilon_{\perp}} & \frac{\sigma_P}{\epsilon_{\perp}} & 0 \\ 0 & 0 & \frac{\sigma_0}{\epsilon_0} \end{bmatrix} \quad (3.18)$$

Using integrating factors, Equation (3.17) gives

$$\underline{\underline{E}} \leftarrow \exp(-\underline{\underline{\Omega}} \delta t) \cdot \underline{\underline{E}} + \delta t \underline{\underline{v}^2} \cdot \exp(-\underline{\underline{\Omega}} \frac{\delta t}{2}) \cdot \underline{\underline{F}} \quad (3.19)$$

TODO: Do we need to be careful here about the difference between a matrix and a tensor?

The tensor exponential can be evaluated by considering the diagonal and off-diagonal terms separately.

$$\underline{\underline{\Omega}} = \underline{\underline{\Omega}}' + \frac{\sigma_H}{\epsilon_{\perp}} \begin{bmatrix} 0 & -1 & 0 \\ 1 & 0 & 0 \\ 0 & 0 & 0 \end{bmatrix} \quad \text{where} \quad \underline{\underline{\Omega}}' = \begin{bmatrix} \frac{\sigma_P}{\epsilon_{\perp}} & 0 & 0 \\ 0 & \frac{\sigma_P}{\epsilon_{\perp}} & 0 \\ 0 & 0 & \frac{\sigma_0}{\epsilon_0} \end{bmatrix} \quad (3.20)$$

Note that tensors are remarkably well-behaved when exponentiated[25]. Because $\underline{\underline{\Omega}}'$ is diagonal, and thus the two commute,

$$\exp(\underline{\underline{T}}) = \sum_n \frac{1}{n!} \underline{\underline{T}}^n \quad \text{and} \quad \exp(\underline{\underline{T}} + \underline{\underline{T}}') = \exp(\underline{\underline{T}}) \exp(\underline{\underline{T}}') \quad (3.21)$$

The off-diagonal terms collapse into sines and cosines, indicating a rotation about z .

$$\underline{\underline{E}} \leftarrow \exp(-\underline{\underline{\Omega}}' \delta t) \cdot \underline{\underline{R}}_z \left(\frac{-\sigma_H \delta t}{\epsilon_{\perp}} \right) \cdot \underline{\underline{E}} + \delta t \underline{\underline{v}^2} \cdot \exp(-\underline{\underline{\Omega}}' \frac{\delta t}{2}) \cdot \underline{\underline{R}}_z \left(\frac{-\sigma_H \delta t}{2\epsilon_{\perp}} \right) \cdot \underline{\underline{F}} \quad (3.22)$$

Where

$$\underline{\underline{R}}_z(\theta) = \begin{bmatrix} \cos \theta & -\sin \theta & 0 \\ \sin \theta & \cos \theta & 0 \\ 0 & 0 & 1 \end{bmatrix} \quad (3.23)$$

The parallel term of term of Equation (3.22) is simply

$$E_{\parallel} \leftarrow E_{\parallel} \exp\left(\frac{-\sigma_0 \delta t}{\epsilon_0}\right) + c^2 \delta t F_{\parallel} \exp\left(\frac{-\sigma_0 \delta t}{2\epsilon_0}\right) \quad (3.24)$$

Or, in covariant terms,

$$E_3 \leftarrow E_3 \exp\left(\frac{-\sigma_0 \delta t}{\epsilon_0}\right) + c^2 \delta t (g_{31} F^1 + g_{33} F^3) \exp\left(\frac{-\sigma_0 \delta t}{2\epsilon_0}\right) \quad (3.25)$$

For the ionospheric profiles and time steps employed by this model, $\frac{\sigma_0 \delta t}{\epsilon_0}$ is never smaller than 10^3 . As a result, $\exp\left(\frac{-\sigma_0 \delta t}{\epsilon_0}\right)$ is far too small to be stored in a double precision variable. That is, this simulation takes E_{\parallel} (and, as a result, E_3) to be uniformly zero.

This, obviously, precludes any discussion of parallel electric fields or parallel currents. These topics are revisited in Chapter 5.

Not unrelatedly, recalling the definition of the plasma frequency and parallel conductivity from Equation (4.5), $\frac{\sigma_0}{\epsilon_0}$ can also be written $\frac{\omega_p^2}{\nu}$.

The plasma frequency is very fast.

The perpendicular components of Equation (3.22), mapped from the physical basis to the contravariant basis (per Equation (3.7)) to the covariant basis (per Equation (3.4)),

give

$$\begin{aligned}
E_1 + \frac{g^{13}}{g^{11}} E_3 &\leftarrow E_1 \cos\left(\frac{-\sigma_H \delta t}{\epsilon_{\perp}}\right) \exp\left(\frac{-\sigma_P \delta t}{\epsilon_{\perp}}\right) \\
&+ E_2 \sin\left(\frac{-\sigma_H \delta t}{\epsilon_{\perp}}\right) \exp\left(\frac{-\sigma_P \delta t}{\epsilon_{\perp}}\right) \sqrt{\frac{g^{22}}{g^{11}}} \\
&+ E_3 \cos\left(\frac{-\sigma_H \delta t}{\epsilon_{\perp}}\right) \exp\left(\frac{-\sigma_P \delta t}{\epsilon_{\perp}}\right) \frac{g^{13}}{g^{11}} \\
&+ F^1 \cos\left(\frac{-\sigma_H \delta t}{2\epsilon_{\perp}}\right) \exp\left(\frac{-\sigma_P \delta t}{2\epsilon_{\perp}}\right) \frac{v_A^2 \delta t}{g^{11}} \\
&+ F^2 \sin\left(\frac{-\sigma_H \delta t}{2\epsilon_{\perp}}\right) \exp\left(\frac{-\sigma_P \delta t}{2\epsilon_{\perp}}\right) \frac{v_A^2 \delta t}{\sqrt{g^{11} g^{22}}}
\end{aligned} \tag{3.26}$$

and

$$\begin{aligned}
E_2 &\leftarrow -E_1 \sin\left(\frac{-\sigma_H \delta t}{\epsilon_{\perp}}\right) \exp\left(\frac{-\sigma_P \delta t}{\epsilon_{\perp}}\right) \sqrt{\frac{g^{11}}{g^{22}}} \\
&+ E_2 \cos\left(\frac{-\sigma_H \delta t}{\epsilon_{\perp}}\right) \exp\left(\frac{-\sigma_P \delta t}{\epsilon_{\perp}}\right) \\
&- E_3 \sin\left(\frac{-\sigma_H \delta t}{\epsilon_{\perp}}\right) \exp\left(\frac{-\sigma_P \delta t}{\epsilon_{\perp}}\right) \frac{g^{13}}{\sqrt{g^{11} g^{22}}} \\
&- F^1 \sin\left(\frac{-\sigma_H \delta t}{2\epsilon_{\perp}}\right) \exp\left(\frac{-\sigma_P \delta t}{2\epsilon_{\perp}}\right) \frac{v_A^2 \delta t}{\sqrt{g^{11} g^{22}}} \\
&+ F^2 \cos\left(\frac{-\sigma_H \delta t}{2\epsilon_{\perp}}\right) \exp\left(\frac{-\sigma_P \delta t}{2\epsilon_{\perp}}\right) \frac{v_A^2 \delta t}{g^{22}}
\end{aligned} \tag{3.27}$$

The E_3 terms can be ignored at present, but Chapter 5 references back to them.

3.4 Driving

If no energy is added, the simulation is pretty boring. Everything just stays zero.

3.4.1 Outer Boundary Compression

Driving from the outer boundary is the traditional way to do it.

TODO: Cite and briefly explain past work done with compressional driving.

As discussed in Section 4.4, Alfvén waves become guided when the azimuthal modenumber is large. The energy all stays close to the outer boundary. No field line resonances of significant strength are created within the magnetosphere.

TODO: Should the model be presented first, or the dispersion relation? It's natural to talk about the ionospheric profiles when presenting the model, which the dispersion relation relies upon. But it's convenient, here, to be able to talk about how Alfvén waves become guided at large m . That probably means that the math should go first, and the ionospheric profiles should be squeezed in somewhere earlier.

Clockwise Toroidal Poynting Flux at 300s: Quiet Day ($\frac{\text{mW}}{\text{m}^2}$)

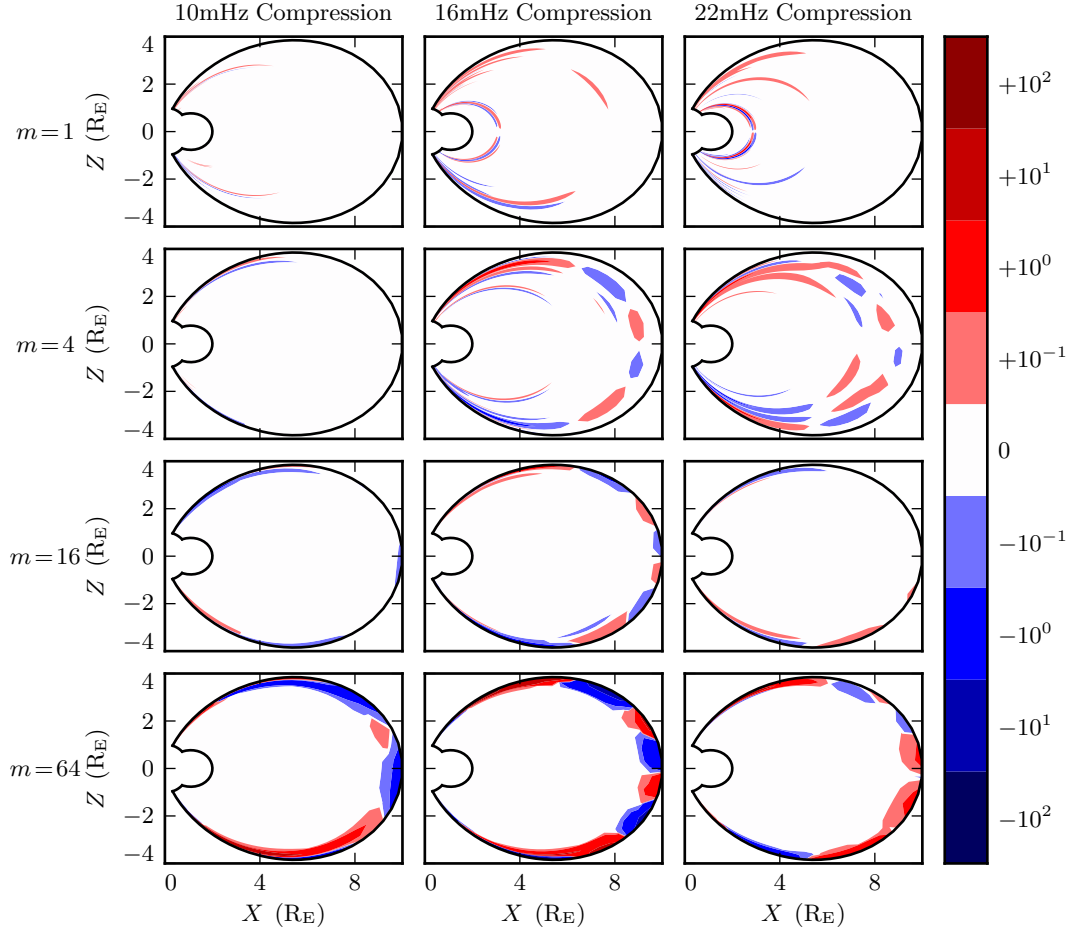


Figure 3.5: When the azimuthal modenumber is small, energy delivered through compression of the outer boundary is able to propagate across field lines and stimulate field line resonances in the inner magnetosphere. However, as modenumber increases, Alfvén waves become increasingly guided. As a result, energy delivered at the outer boundary cannot penetrate to the inner magnetosphere. Note that the large values on the bottom row should be taken with a grain of salt; it's not clear that the simulation is reliable when waves are continuously forced against the boundary.

Compressional driving is applied by setting the value of B_3 at the outer boundary.

A compression might reasonably be expected to drive waves with long azimuthal wavelengths. However, there is some indication that waves with short azimuthal wavelength can be driven as well, such as through Kelvin-Helmholtz interactions.

TODO: Find this claim again and cite it.

3.4.2 Ring Current Modulation

Pc4 pulsations with high azimuthal modenumber are known to be driven from within the magnetosphere, such as through drift-resonant interactions with energetic radiation belt and ring current particles.

TODO: Cite.

Substorm injection can cause localized ring current behavior.

TODO: UNH was looking at this at AGU. Check if they have published yet.

During geomagnetically active times, the ring current is a dynamic region. It's easy to imagine localized perturbations.

It's difficult to estimate how large such perturbations might be. The following is a kludgey estimate.

Sym-H Frequency Breakdown for June 2013 Storm

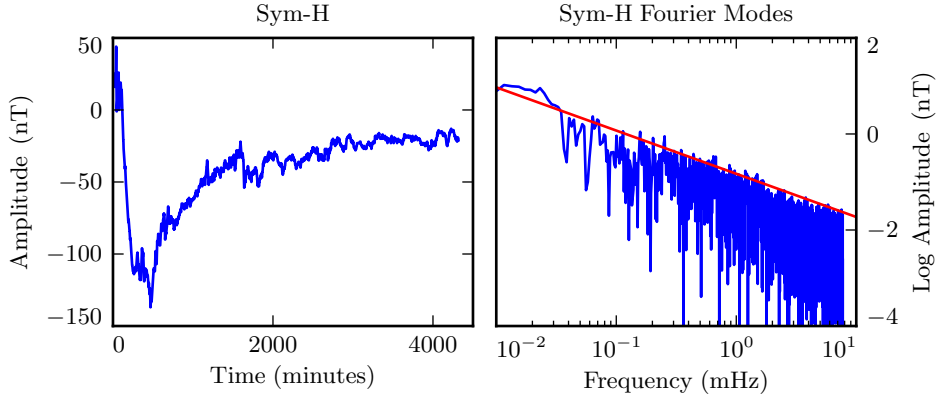


Figure 3.6: The Sym-H storm index (from NASA CDAWeb[26]) measures magnetic perturbations on Earth’s surface due to ring current activity. It is measured once per minute, so Fourier amplitudes in the Pc4 range cannot be measured directly. However, they can be inferred by fitting the pink noise. The red line shows a fit to the top of the distribution, $\sim 10^{-2}$ nT $\left(\frac{20 \text{ mHz}}{f}\right)$.

Sym-H is like Dst, but with greater time resolution.

The noise suggests that a Fourier component with a period of about 1 min could have an amplitude around 10^{-2} nT.

If the driving is delivered at $L = 5$, with a standard deviation of $0.5 R_E$ in the radial direction and 5° angularly, that corresponds to a current density on the order of $10^{-4} \mu\text{A}/\text{m}^2$. This comes from approximating the ring current as a ring of current. Of course, Sym-H is measured at Earth’s surface, not at the center of the ring; this gives a geometric factor of about two.

TODO: What electric field magnitude does this correspond to?

Current driving is applied by adding an additional current term. Ampère's Law becomes

$$\underline{\epsilon} \cdot \frac{\partial}{\partial t} \underline{E} = \frac{1}{\mu_0} \nabla \times \underline{B} - \underline{\sigma} \cdot \underline{E} - \underline{J}_{drive} \quad (3.28)$$

And this driving term is absorbed into the curl by revising Equation (3.13) from $\underline{F} \equiv \nabla \times \underline{B}$ to $\underline{F} \equiv \nabla \times \underline{B} - \underline{J}_{drive}$. (As a result, Equations (3.26) and (3.27) do not change.)

Notably, Sym-H is a global quantity; it's not ideally suited for making estimates of localized inhomogeneity.

Furthermore, Sym-H has a time resolution of 1 min. It can hardly be said to carry information about oscillations at frequencies of less than two minutes.

Sym-H gives no way to estimate azimuthal modenumber. That's based on Pc4 observations. Dai[5] observed modenumbers approaching 100.

A kludgey estimate is better than no estimate.

3.5 Boundary Conditions

The grid can't go on forever. There have to be special cases at the edges.

3.5.1 Parity and Interpolation

Computation takes place on a staggered grid.

Field values are offset to ensure that most differences are centered. For example, $\frac{\partial}{\partial t} B_2$ depends on $\frac{\partial}{\partial u^1} E_3$ and $\frac{\partial}{\partial u^3} E_1$. If B_2 is defined at even i , E_3 is defined at odd i , so that B_2 is defined on the same grid points as $\frac{E_3[i+1]-E_3[i-1]}{u^1[i+1]-u^1[i-1]}$.

TODO: Make sure the example uses the correct parities.

TODO: Find a citation for the wiggles that occur if field values are defined on all grid points, due to the weak coupling. This problem is apparently well-known.

Values are sometimes needed off-parity. E_1 and E_2 are not defined at the same grid locations, but they are coupled directly by the Hall conductivity. And B_1 and B_3 are coupled by the non-orthogonality of the grid. When off-parity values are needed, they are interpolated from their neighbors.

Differentiation and interpolation are good to second order on the nonuniform grid. Like the coefficients for Maxwell's equations, differentiation and interpolation weights are computed during setup to save time during iteration.

Electric fields go to zero at the innermost and outermost field lines (Dirichlet boundary conditions). Magnetic fields have zero derivative (Neumann boundary conditions). For components not defined at the exact boundary, these rules are applied when differentiating or interpolating; they set the effective value just outside the grid.

These boundary conditions can in principle cause nonphysical reflection at the boundary. In practice, that is not an issue. Wave activity is concentrated well away from the boundaries. In fact, reversing the Dirichlet and Neumann boundary conditions has little effect.

(Of course, an inconsistent boundary condition – like using the same boundary condition for a field and its derivative – causes instability.)

3.5.2 Coupling to the Atmosphere

Conditions at the ionospheric boundaries are set by coupling to the atmosphere. This also allows the computation of ground fields.

It's reasonable to approximate the atmosphere as a perfect insulator, giving $\nabla \times \underline{B} = 0$. Combining with $\nabla \cdot \underline{B} = 0$ per Maxwell's equations, ensures the existence of a scalar magnetic potential Ψ such that $\underline{B} = \nabla \Psi$ and Ψ satisfies Laplace's equation, $\nabla^2 \Psi = 0$.

Laplace's equation can be solved analytically; in spherical coordinates, the solutions are spherical harmonics. However, a numerical solution is preferable to ensure orthonormality on a discrete (and incomplete – there are no grid points at the poles or equator) grid. After separating out the radial and azimuthal dependence in the usual way, the

latitudinal component of Laplace's equation (in terms of $s \equiv -\sin^2 \theta$) is

$$(4s^2 + 4s) \frac{d^2}{ds^2} Y_\ell + (4 + 6s) \frac{d}{ds} Y_\ell - \frac{m^2}{s} Y_\ell = \ell(\ell + 1) Y_\ell \quad (3.29)$$

Using centered differences to express the derivatives, Equation (3.29) is a system of linear equations, one per field line. It can be solved numerically for eigenvalues $\ell(\ell + 1)$ and eigenvectors (harmonics) Y_ℓ . In terms of those harmonics, and noting that the model uses a fixed azimuthal modenumber m , Ψ between R_E and R_I can be expressed

$$\Psi(r, \theta, \phi) = \sum_\ell \left(\alpha_\ell r^\ell + \beta_\ell r^{-\ell-1} \right) Y_\ell(\theta) \exp(im\phi) \quad (3.30)$$

As a boundary condition for Ψ , Earth's crust is assumed to be a perfect conductor, forcing the magnetic field at the boundary to be perfectly horizontal. That is, $B_r = \frac{\partial}{\partial r} \Psi = 0$. Then, noting that the harmonics Y_ℓ are orthonormal (so each term of the sum must be zero),

$$\beta_\ell = \frac{\ell}{\ell + 1} R_E^{2\ell+1} \alpha_\ell \quad (3.31)$$

Note that the explicit ϕ dependence has been dropped. The entire simulation shares a fixed modenumber, so it's sufficient to find Ψ at $\phi = 0$.

At the top of the atmosphere, the radial magnetic field is again used as a boundary condition, this time to compute the weights α_ℓ .

TODO: Something something thin horizontal current sheet at R_I .

Taking the shorthand $\lambda_I \equiv \frac{R_E}{R_I} \sim 0.975$

$$B_r = \sum_\ell \ell \alpha_\ell R_I^{\ell-1} \left(1 - \lambda_I^{2\ell-1} \right) Y_\ell \quad (3.32)$$

TODO: Settle on good notation for taking the inner product of harmonics. It's a vector in the sense that it's a one-dimensional array of values, but not in the physical sense. Indexing – $B_r [i]$ – also seems awkward.

The sum can be collapsed by “integrating” over a harmonic. The inverse harmonics are obtained by inverting the eigenvector matrix. Then $Y_\ell \cdot Y_{\ell'}^{-1} = \delta_{\ell\ell'}$ by construction.

$$\alpha_\ell = \frac{1}{\ell R_I^{\ell-1}} \frac{B_r \cdot Y_\ell^{-1}}{1 + \lambda_I^{2\ell+1}} \quad (3.33)$$

Combining Equations (3.30), (3.31), and (3.33) allows the expression of Ψ at the top and bottom of the atmosphere as a linear function of the radial magnetic field at the boundary.

$$\begin{aligned} \Psi_E &= \sum_\ell Y_\ell \frac{R_I}{\ell} \frac{\frac{2\ell-1}{\ell-1} \lambda^\ell}{1 - \lambda_I^{2\ell+1}} B_r \cdot Y_\ell^{-1} \\ \Psi_I &= \sum_\ell Y_\ell \frac{R_I}{\ell} \frac{1 + \frac{\ell}{\ell-1} \lambda_I^{2\ell+1}}{1 - \lambda_I^{2\ell+1}} B_r \cdot Y_\ell^{-1} \end{aligned} \quad (3.34)$$

Magnetic fields are evaluated from Ψ per

$$B_1 = \frac{\partial}{\partial u^1} \Psi \quad B_2 = \frac{\partial}{\partial u^2} \Psi \quad (3.35)$$

Note that B_1 and B_2 are horizontal; per Equation (3.8), they are proportional to B_θ and B_ϕ respectively.

At the ground, field values are purely output.

Horizontal magnetic field values at the top of the ionosphere, on the other hand, are used as boundary conditions. Assuming there is no vertical component to the ionospheric current sheet, the electric field values at the ionospheric edge of the grid are dictated by the jump in horizontal magnetic field between the bottom of the grid and the top of the atmosphere.

$$\mu_0 \underline{\underline{\Sigma}} \cdot \underline{E} = \lim_{\delta r \rightarrow 0} \hat{r} \times \underline{B} \Big|_{R_I - \delta r}^{R_I + \delta r} \quad (3.36)$$

TODO: Bob’s citations for the ionospheric jump conditions: Fujita and Tamao 1988, Yosikawa and Itonaga 1996, 2000, Lysak and Song 2001, Sciffer and Waters 2002. It

basically comes from integrating Ampère's Law, so half a dozen citations seems like overkill.

The harmonic breakdown of Ψ also allows for the calculation of how much energy is leeched by the atmosphere.

$$B_r = \frac{\partial}{\partial r} \Psi \quad B_\theta = \frac{1}{r} \frac{\partial}{\partial \theta} \Psi \quad B_\phi = \frac{1}{r \sin \theta} \frac{\partial}{\partial \phi} \Psi \quad (3.37)$$

TODO: Plug Equations (3.30) and (3.31) into these expressions, then that into $u = \frac{1}{2\mu_0} |\underline{B}|^2$, then integrate from R_E to R_I and in angle.

Chapter 4

Waves in Cold Resistive Plasmas

TODO: This chapter works out the sorts of waves that might be expected in the numerical model. It starts with the same equations that are used by the model – Maxwell’s equations and Ohm’s Law. The resulting dispersion relation is too high-ordered for a direct solution, so several limits of interest are considered.

TODO: At this end of this chapter, there will be a discussion of what is specifically interesting about the findings. That doesn’t really exist yet.

Cold, linearized Ampère’s Law and Faraday’s Law. The vector \underline{B} is the perturbation to the zeroth-order magnetic field.

$$\frac{\partial}{\partial t} \underline{B} = -\nabla \times \underline{E} \quad \underline{\epsilon} \cdot \frac{\partial}{\partial t} \underline{E} = \frac{1}{\mu_0} \nabla \times \underline{B} - \underline{J} \quad (4.1)$$

Ohm’s Law. Electron inertial effects are included in the parallel direction. See Chapter 5.

$$\frac{m_e}{ne^2} \frac{\partial}{\partial t} J_{\parallel} = \sigma_0 E_{\parallel} - J_{\parallel} \quad 0 = \underline{\sigma}_{\perp} \cdot \underline{E}_{\perp} - \underline{J}_{\perp} \quad (4.2)$$

Suppose that the fields and currents are resonating as $\exp(i\underline{k} \cdot \underline{x} - i\omega t)$. Evaluate the

derivatives. Eliminate magnetic fields and currents.

$$0 = E_{\parallel} + \frac{c^2}{\omega^2} (\underline{k} \cdot \underline{E} - k^2 \underline{E})_{\parallel} + \frac{i\omega_P^2}{\omega(\nu - i\omega)} E_{\parallel} \quad (4.3)$$

$$0 = \underline{E}_{\perp} + \frac{v_A^2}{\omega^2} (\underline{k} \cdot \underline{E} - k^2 \underline{E})_{\perp} + \frac{i}{\epsilon_{\perp}\omega} \underline{\sigma}_{\perp} \cdot \underline{E}_{\perp} \quad (4.4)$$

The above expression makes use of the vector identity $\underline{k} \times \underline{k} \times \underline{E} = \underline{k} \underline{k} \cdot \underline{E} - k^2 \underline{E}$. The Alfvén speed, speed of light, plasma frequency, and parallel conductivity are defined in the usual way:

$$v_A^2 \equiv \frac{1}{\mu_0 \epsilon_{\perp}} \quad c^2 \equiv \frac{1}{\mu_0 \epsilon_0} \quad \omega_P^2 \equiv \frac{ne^2}{m_e \epsilon_0} \quad \sigma_0 \equiv \frac{ne^2}{m_e \nu} \quad (4.5)$$

Note that this definition of the Alfvén speed takes into account the displacement current correction which is important when v_A approaches c .

Without loss of generality, the wave vector \underline{k} can be said to lie in the x - z plane; the distinction between the x and y directions is revisited in Section 4.4. Let θ be the angle between \underline{k} and the zeroth-order magnetic field.

Then Equations (4.3) and (4.4) can be combined into the usual dispersion tensor form, $\underline{\underline{T}} \cdot \underline{E} = 0$, where

$$\underline{\underline{T}} = \underline{\underline{\mathbb{I}}} + \frac{k^2}{\omega^2} \begin{bmatrix} -v_A^2 \cos^2 \theta & 0 & v_A^2 \sin \theta \cos \theta \\ 0 & -v_A^2 & 0 \\ c^2 \sin \theta \cos \theta & 0 & -c^2 \sin^2 \theta \end{bmatrix} + \frac{i}{\omega} \begin{bmatrix} \frac{\sigma_P}{\epsilon_{\perp}} & -\frac{\sigma_H}{\epsilon_{\perp}} & 0 \\ \frac{\sigma_H}{\epsilon_{\perp}} & \frac{\sigma_P}{\epsilon_{\perp}} & 0 \\ 0 & 0 & \frac{\omega_P^2}{\nu - i\omega} \end{bmatrix} \quad (4.6)$$

Nontrivial solutions exist only when $|\underline{\underline{T}}| = 0$. This gives rise to a seventh-order polynomial in ω , so it's necessary to consider limits of particular interest.

4.1 Parallel Propagation Limit

Parallel propagation is a naive representation of a field line resonance; the wave vector moves energy along the field line. Taking $\theta = 0$, $\underline{\underline{T}}$ simplifies to

$$\underline{\underline{T}}_{\parallel} = \underline{\underline{\mathbb{I}}} - \frac{k^2 v_A^2}{\omega^2} \begin{bmatrix} 1 & 0 & 0 \\ 0 & 1 & 0 \\ 0 & 0 & 0 \end{bmatrix} + \frac{i}{\omega} \begin{bmatrix} \frac{\sigma_P}{\epsilon_{\perp}} & -\frac{\sigma_H}{\epsilon_{\perp}} & 0 \\ \frac{\sigma_H}{\epsilon_{\perp}} & \frac{\sigma_P}{\epsilon_{\perp}} & 0 \\ 0 & 0 & \frac{\omega_P^2}{\nu - i\omega} \end{bmatrix} \quad (4.7)$$

Conveniently, parallel and perpendicular polarizations are not coupled in Equation (4.7).

4.1.1 Parallel Polarization

The parallel component of the determinant of Equation (4.7) gives

$$\omega^2 + i\nu\omega - \omega_P^2 = 0 \quad (4.8)$$

With no k dependence this expression doesn't describe a wave per se, so much as a resonant frequency. Solving directly,

$$\omega = -\frac{i\nu}{2} \pm \sqrt{\omega_P^2 - \frac{\nu^2}{4}} \quad (4.9)$$

The plasma frequency significantly exceeds the collision frequency everywhere except a narrow strip at the ionospheric boundary of the model. Expanding in large ω_P gives

$$\omega^2 = \omega_P^2 - i\nu\omega_P + \dots \quad (4.10)$$

TODO: Actually, double-check this. How does ν compare to ω_P at the ionospheric boundary when there is no Boris factor?

This is the plasma oscillation.

4.1.2 Perpendicular Polarization

The perpendicular components of the determinant of Equation (4.7) give

$$\omega^4 + 2i\frac{\sigma_P}{\epsilon_\perp}\omega^3 - \left(2k^2v_A^2 + \frac{\sigma_P^2 + \sigma_H^2}{\epsilon_\perp^2}\right)\omega^2 - 2ik^2v_A^2\frac{\sigma_P}{\epsilon_\perp}\omega + k^4v_A^4 = 0 \quad (4.11)$$

This can be solved in exact form. Noting that \pm and \oplus are independent,

$$\omega = \left(\frac{\pm\sigma_H - i\sigma_P}{2\epsilon_\perp}\right) \oplus \sqrt{k^2v_A^2 + \left(\frac{\pm\sigma_H - i\sigma_P}{2\epsilon_\perp}\right)^2} \quad (4.12)$$

Over the vast majority of a field line, $kv_A \gg \frac{\sigma_P}{\epsilon_\perp}$ and $kv_A \gg \frac{\sigma_H}{\epsilon_\perp}$.

$$\omega^2 = k^2v_A^2 \oplus kv_A\frac{\sigma_H \pm i\sigma_P}{\epsilon_\perp} + \dots \quad (4.13)$$

This is the Alfvén wave, evidently split by the ionospheric conductivity, propagating along the zeroth-order magnetic field line.

4.2 Perpendicular Propagation Limit

A wave's ability to propagate across field lines is also of interest. When $\theta = \frac{\pi}{2}$, \underline{T}_\perp simplifies to

$$\underline{T}_\perp = \underline{\underline{I}} - \frac{k^2}{\omega^2} \begin{bmatrix} 0 & 0 & 0 \\ 0 & v_A^2 & 0 \\ 0 & 0 & c^2 \end{bmatrix} + \frac{i}{\omega} \begin{bmatrix} \frac{\sigma_P}{\epsilon_\perp} & -\frac{\sigma_H}{\epsilon_\perp} & 0 \\ \frac{\sigma_H}{\epsilon_\perp} & \frac{\sigma_P}{\epsilon_\perp} & 0 \\ 0 & 0 & \frac{\omega_P^2}{\nu - i\omega} \end{bmatrix} \quad (4.14)$$

As in the parallel propagation case, the parallel and perpendicular components of the determinant are decoupled.

4.2.1 Parallel Polarization

The parallel component of the determinant of Equation (4.14) gives

$$\omega^3 + i\nu\omega^2 - (k^2c^2 + \omega_P^2)\omega - ik^2c^2\nu = 0 \quad (4.15)$$

The above expression can be solved exactly, but the resulting expressions are too long to be useful.

Expanding the solution in large ω_P gives the O mode: a compressional wave with a parallel electric field.

$$\omega^2 = k^2c^2 + \omega_P^2 - i\nu\omega_P + \dots \quad (4.16)$$

4.2.2 Perpendicular Polarization

The perpendicular components of the determinant of Equation (4.14) give

$$\omega^3 + 2i\frac{\sigma_P}{\epsilon_\perp}\omega^2 - \left(2k^2v_A^2 + \frac{\sigma_P^2 + \sigma_H^2}{\epsilon_\perp^2}\right)\omega - ik^2v_A^2\frac{\sigma_P}{\epsilon_\perp} = 0 \quad (4.17)$$

Again, the roots of the cubic are impractically long.

Expanding in large conductivity, as is expected near the ionospheric boundary, gives

$$\omega^2 = k^2v_A^2 + \left(\frac{\sigma_H \pm i\sigma_P}{\epsilon_\perp}\right)^2 + \dots \quad (4.18)$$

Whereas expanding in small conductivity, as is expected far from the boundary, gives

$$\omega^2 = k^2v_A^2 \pm ikv_A\frac{\sigma_P}{\epsilon_\perp} + \dots \quad (4.19)$$

Both of which are Alfvén waves.

4.3 High Altitude Limit

At high altitude, where the density is very low compared to the ionosphere, it's reasonable to approximate $\sigma_P \rightarrow 0$ and $\sigma_H \rightarrow 0$ and $\nu \rightarrow 0$.

In this case, $\underline{\underline{T}}$ simplifies to

$$\underline{\underline{T}}_\infty = \underline{\underline{\mathbb{I}}} - \frac{k^2}{\omega^2} \begin{bmatrix} v_A^2 \cos^2 \theta & 0 & -v_A^2 \sin \theta \cos \theta \\ 0 & v_A^2 & 0 \\ -c^2 \sin \theta \cos \theta & 0 & c^2 \sin^2 \theta \end{bmatrix} - \frac{\omega_P^2}{\omega^2} \begin{bmatrix} 0 & 0 & 0 \\ 0 & 0 & 0 \\ 0 & 0 & 1 \end{bmatrix} \quad (4.20)$$

In this case it's the azimuthal polarization that decouples from the other two.

4.3.1 Azimuthal Polarization

The azimuthal component of the determinant of Equation (4.20) simply gives the Alfvén wave.

$$\omega^2 = k^2 v_A^2 \quad (4.21)$$

4.3.2 Meridional Polarization

The components of the determinant of Equation (4.20) which fall in the meridional plane give, taking $k_\perp \equiv k \sin \theta$ and $k_\parallel \equiv k \cos \theta$,

$$\omega^4 - \left(k_\parallel^2 v_A^2 + k_\perp^2 c^2 + \omega_P^2 \right) \omega^2 + k_\parallel^2 v_A^2 \omega_P^2 = 0 \quad (4.22)$$

The above expression is quadratic in ω^2 , and thus can be solved directly.

$$\omega^2 = \frac{1}{2} \left(k_\parallel^2 v_A^2 + k_\perp^2 c^2 + \omega_P^2 \right) \pm \sqrt{\frac{1}{4} \left(k_\parallel^2 v_A^2 + k_\perp^2 c^2 + \omega_P^2 \right)^2 - k_\parallel^2 v_A^2 \omega_P^2} \quad (4.23)$$

Noting that ω_P is very large, the two roots simplify to

$$\omega^2 = k_{\parallel}^2 v_A^2 + \dots \quad (4.24)$$

$$\omega^2 = k_{\parallel}^2 v_A^2 + k_{\perp}^2 c^2 + \omega_P^2 + \dots \quad (4.25)$$

4.4 Implications for This Work

4.4.1 Mode Coupling

TODO: Have we got enough/appropriate math here to talk about how σ_H rotates fields at the ionosphere? Doubtful.

4.4.2 High Modenumber Cutoff

As m becomes large, it puts a lower bound on the modenumber, and thus on the frequency. For an Alfvén wave, $\omega^2 = k^2 v_A^2$,

$$k \geq k_{\phi} = \frac{m}{2\pi r} \quad \text{so} \quad \omega \geq \frac{m}{2\pi r} v_A \quad (4.26)$$

Any wave with a frequency below this threshold will become evanescent.

TODO: This point is pretty important. It's revisited in Section 3.4.

Chapter 5

Electron Inertial Effects

TODO: Note that Bob's 2011 paper[27] had inertial effects.

The model described in Chapter 3 has the notable omission of parallel electric fields and parallel currents. That situation can be remedied by the addition of the electron inertial term in Ohm's Law.

Old parallel electric field formulation. Recall $\underline{F} \equiv \nabla \times \underline{B}$.

$$\epsilon_0 \frac{\partial}{\partial t} E_{\parallel} = \frac{1}{\mu_0} F_{\parallel} - \sigma_0 E_{\parallel} \quad (5.1)$$

New parallel electric field formulation. The parallel current must now be tracked explicitly.

$$\epsilon_0 \frac{\partial}{\partial t} E_{\parallel} = \frac{1}{\mu_0} F_{\parallel} - J_{\parallel} \quad \frac{\partial}{\partial t} J_{\parallel} = \frac{ne^2}{m} E_{\parallel} - \nu J_{\parallel} \quad (5.2)$$

In the new formulation, J_{\parallel} (proportional to J_3) is solved with integrating factors and E_{\parallel} (E_3) can be advanced directly.

$$\begin{aligned} E_3 &\leftarrow E_3 + c^2 \delta t (g_{31} F^1 + g_{33} F^3) - \frac{\delta t}{\epsilon_0} J_3 \\ J_3 &\leftarrow J_3 \exp(-\nu \delta t) + \frac{ne^2}{m} \delta t E_3 \exp(-\nu \frac{\delta t}{2}) \end{aligned} \quad (5.3)$$

Recall that the electric and magnetic fields are staggered by half a time step. The current is defined with the magnetic fields, offset from the electric fields.

5.1 The Boris Approximation

Note that

$$\frac{\partial}{\partial t} E_{\parallel} \sim -\frac{1}{\epsilon_0} J_{\parallel} \quad \text{and} \quad \frac{\partial}{\partial t} J_{\parallel} \sim \frac{ne^2}{m_e} E_{\parallel} \quad \text{so} \quad \frac{\partial^2}{\partial t^2} E_{\parallel} \sim -\omega_P^2 E_{\parallel} \quad (5.4)$$

That is, the addition of the electron inertial term in Ohm's Law allows plasma oscillations.

As noted in Section 3.3.3, the plasma frequency is very large. Much larger than $\frac{1}{\delta t}$. But $\omega_P \delta t < 1$ is necessary for stability. In order to accommodate that condition, the time step in some runs would need to be dropped by three orders of magnitude; a simulation slated for one hour would suddenly take six weeks to complete.

The time step dictated by the Alfvén speed and grid spacing is typically on the order of 10 μs , while the plasma frequency can be as small as 10 ns.

The plasma frequency (and the speed of light) can be decreased by taking an artificially large value for ϵ_0 . Such approximations have been staples of numerical MHD models since Boris' work in 1970[28].

Lysak and Song[29] demonstrate the validity of such an approximation. To paraphrase their work, take Equation (5.2) and suppose that E_{\parallel} and J_{\parallel} are oscillating at a frequency ω . Then,

$$-i\omega\epsilon_0 E_{\parallel} = \frac{1}{\mu_0} F_{\parallel} - J_{\parallel} \quad -i\omega J_{\parallel} = \frac{ne^2}{m_e} E_{\parallel} - \nu J_{\parallel} \quad (5.5)$$

So

$$\left(1 - \frac{\omega^2 - i\nu\omega}{\omega_P^2}\right) E_{\parallel} = \frac{c^2}{\omega_P^2} (\nu - i\omega) F_{\parallel} \quad (5.6)$$

Here $\frac{c}{\omega_P}$ is the electron inertial length. While the speed of light and the plasma frequency each depend on ϵ_0 , their ratio does not. So long as $\left(1 - \frac{\omega^2 - i\nu\omega}{\omega_P^2}\right) \sim 1$, a change in ϵ_0 should not affect model behavior.

For the purposes of simulating ultra low frequency waves, Equation (5.6) allows perhaps-implausibly large Boris factors; even increasing ϵ_0 by a factor of 10^6 gives $\left|\frac{\omega^2 + i\omega\nu}{\omega_P^2}\right| \lesssim 0.01$. At that point, in some places, the speed of light is significantly slower than the Alfvén speed.

TODO: Ronnmark[30] calls this “anisotropic vacuum.”

TODO: Plot of these frequency ratios in the ionosphere?

TODO: Generalized Ohm’s Law, in case we decide we need it. Could talk through why all of the other terms are OK to neglect.

$$\underline{E} + \underline{U} \times \underline{B} = \eta \underline{J} + \frac{m_e}{ne^2} \left[\frac{\partial}{\partial t} \underline{J} + \nabla \cdot (\underline{J} \underline{U} + \underline{U} \underline{J} + \frac{1}{ne} \underline{J} \underline{J}) \right] + \frac{1}{ne} \underline{J} \times \underline{B} - \frac{1}{ne} \nabla \cdot \underline{\underline{P}_e} \quad (5.7)$$

5.2 Effect on the Simulation

Magnetic Fields from 300s of 16mHz Current: Active Day, $m = 4$

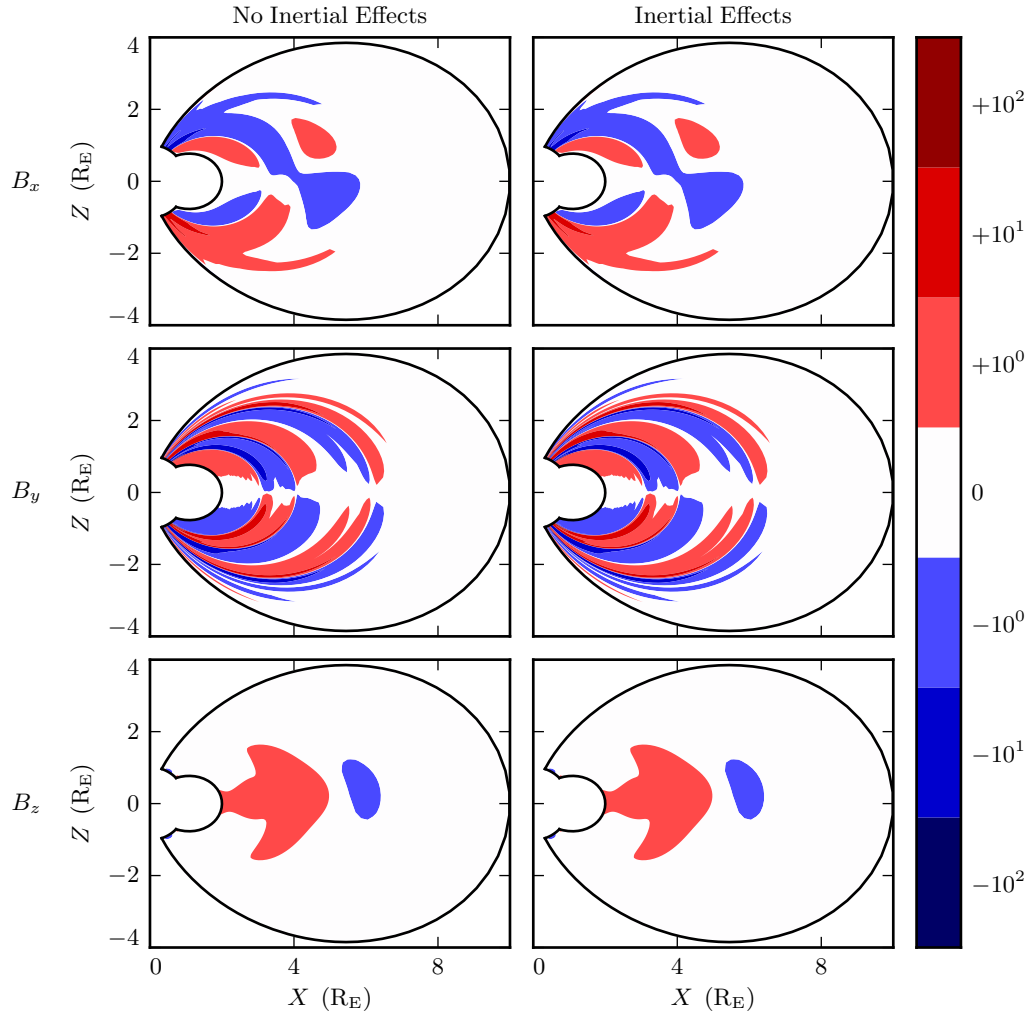


Figure 5.1: The addition of electron inertial effects, with no other changes to the model, does not visible change the output. In a way, this is reassuring, since the alternative is to cast doubt on past work.

5.3 Field-Aligned Current

Over the bulk of the simulation, each field is overwhelmingly real or imaginary. Driving is injected into the real poloidal electric field, giving real E_x and B_y (and real B_z , at least for low m ... at large m , the compressional magnetic field becomes very small). Toroidal components – E_x and B_y – are imaginary, indicating an azimuthal offset.

This comes from the curls in Faraday's Law and Ampère's Law; a derivative in the azimuthal direction comes with a factor of i .

By that reasoning, it seems that the parallel electric field E_z should line up with the toroidal mode.

The distinction between real and imaginary fields gets muddled at the ionosphere, since (imaginary) E_x and (real) E_y are coupled by the Hall conductivity.

The finer points are still being worked out.

Field-Aligned Current and Poynting Flux at R_I : Active Day, 16mHz Current

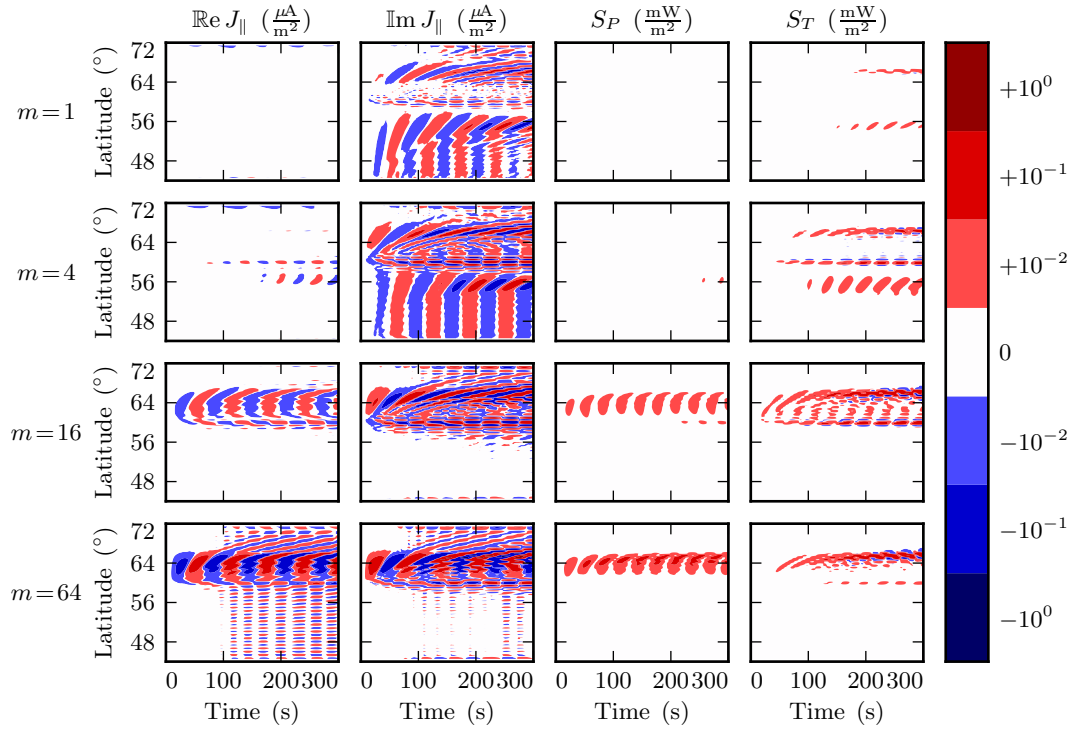


Figure 5.2: Perhaps unsurprisingly, field-aligned current structures at the ionospheric boundary line up with Poynting flux structures. The imaginary component of the current lines up with the (imaginary) toroidal Poynting flux, while the real current lines up with the poloidal Poynting flux.

TODO: Notably, while the net Poynting flux is downward almost everywhere, field-aligned currents alternate between upward and downward flow. Perhaps this has to do with Poynting flux being a quadratic quantity while current is linear? Check the phases of the electric and magnetic fields.

The “wiggles” visible in the lower-left corner of Figure 5.2 suggests overcorrection due to an improperly-coarse grid. See Section 5.4.

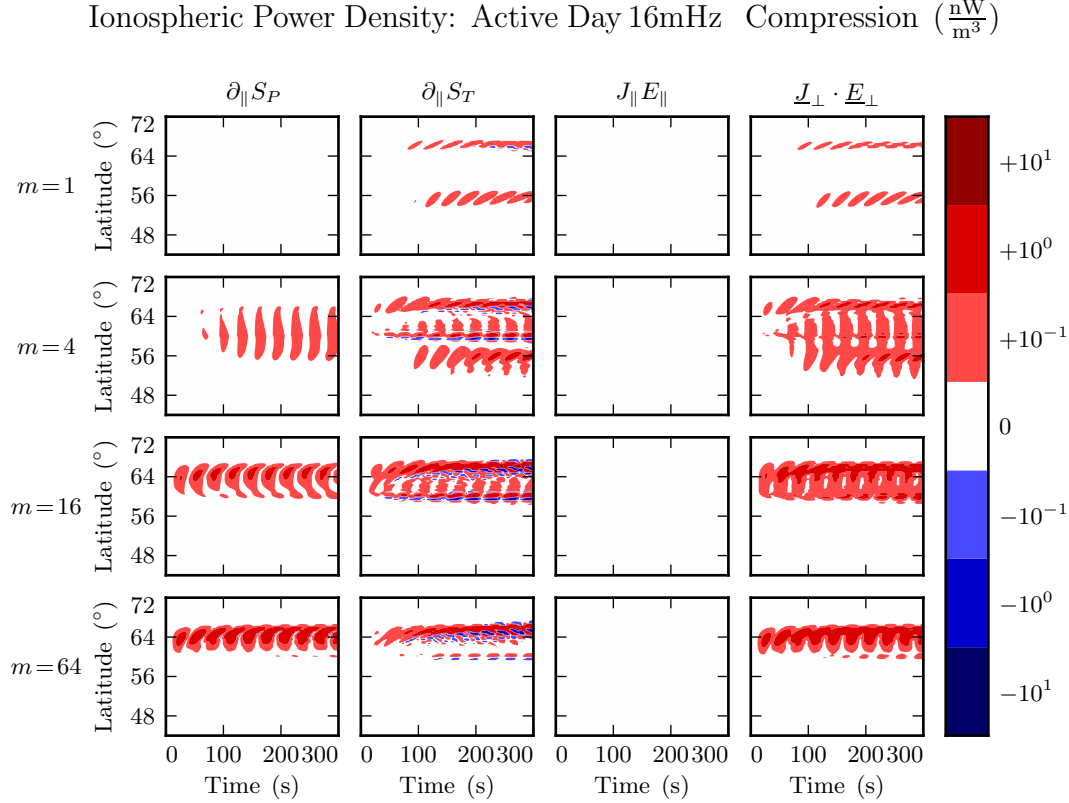


Figure 5.3: While field-aligned currents can be of significant size, they are not particularly good at depositing energy in the ionosphere. Energy deposited by the Poynting flux matches closely with Joule dissipation from the perpendicular currents – energy conservation! – while $J_{\parallel} E_{\parallel}$ is smaller by several orders of magnitude.

5.4 Inertial Length Scales

A typical run has maximum E_y on the order of 10 mV/m and maximum E_z on the order of 10^{-3} mV/m. Notably, however, it's the electric field derivative that affects the magnetic field, not its magnitude.

At the ionospheric boundary, signatures in E_y can vary on length scales of about 1° . This gives $\frac{\partial}{\partial x} E_y \delta t \sim 10^{-3}$ nT/s.

The usual grid can't resolve features much smaller than that. But, recall from Section 5.1, that simulations now include plasma oscillation, for which the characteristic length scale is the electron inertial length, $\frac{c}{\omega_p}$.

The electron inertial length bottoms out below 10^{-1} km inside the plasmasphere, and 1 km outside it.

The very small E_z values being seen are unlikely to dominate E_x , but if inertial length scales were resolved in the perpendicular direction then $\frac{\partial}{\partial x} E_z \delta t$ could be as large as 10^{-4} nT/s.

Resolving electron inertial lengths is computationally very expensive.

The range of L values is decreased from $2R_E$ to $10R_E$ down to $5R_E$ to $7R_E$. The number of grid points in the perpendicular direction is increased by a factor of five. This drops the time step by an order of magnitude – smaller zones have smaller crossing times!

All in all, a run that resolves inertial length scales is a factor of 100 more expensive than one that doesn't.

TODO: Several such runs are going right now. They should finish over the weekend. Then we can see what our tiny grid spacing buys us!

Chapter 6

Comparison to Van Allen Probes

TODO: I have met a handful of times with John (Wygant) to discuss how to get some RBSP data into this dissertation.

TODO: John has recently become interested in the long (26 d or so) cycle in the size of the plasmapause.

TODO: Lei recently compiled a list of several hundred Pc4 events seen by RBSP[5]. He binned them by plasmapause location, noting that there were a significant number of events in the entire interval $4 \lesssim L \lesssim 6$. However, he was just writing about occurrence rate, so he didn't delve into how the large-plasmasphere Pc4s were different from the small-plasmasphere ones.

TODO: I'll bet I can find a pattern or two in Pc4 behavior based on plasmapause location. It'll be interesting to see if the model exhibits the same pattern as the plasmapause location is adjusted.

TODO: I emailed Lei about this earlier this week. He sent over his event list.

TODO: Sheng has agreed to show me how to access RBSP data.

TODO: There is some concern about the rules attached to funding. Apparently NASA fundees aren't allowed to be involved in two-person collaborations with international scientists, or something? We'll have to get that figured out.

Chapter 7

Large Modenumber Effects

This chapter is the real moneymaker.

The overarching motivation for this work is that Pc4 pulsations vary in interesting ways with respect to azimuthal modenumber, and that prior models have been unable to give a good picture of that behavior.

7.1 Finite Poloidal Lifetimes

Radoski[12] looked at Alfvén waves, using a cylindrical coordinate system to imitate an “unwrapped” dipole. He argued that poloidal waves should asymptotically rotate to the toroidal mode.

Mann[13] performed some wave-in-a-box simulations and found the rotation time to be linear in modenumber: $\tau = \frac{d\lambda}{d\omega'_A}$, where $\lambda = \frac{m}{2\pi r}$ and ω'_A is the spatial derivative of the Alfvén bounce frequency. Soon afterwards[14], he supported his simulations analytically.

TODO: Crunch out $\frac{d\lambda}{d\omega'_A}$. Preliminary indications are that it doesn’t translate well to a realistic grid, but let’s double check.

Ding[31] ran simulations more-or-less concurrent with Mann’s. Ding saw a rotation from poloidal to toroidal... then back again. It seems that the reversal was a spatial

resolution issue.

The aforementioned models made significant simplifying assumptions in terms of geometry and boundary conditions.

Mann used straight field lines, a uniform Alfvén speed gradient, and perfectly conducting boundaries.

Ding's simulation is nominally carried out in a dipole geometry, but the ionospheric boundary is at $2.5 R_E$. Boundaries are also perfectly conducting.

That is, the results below offer a significantly higher level of realism than any past simulation (in part, of course, because computers are a lot better than they were 20 years ago).

A dedicated 3D treatment of this problem is unlikely at present. Large azimuthal modenumbers are expensive to compute. That's the whole point!

The energy is obtained by integrating (using the Jacobian to handle the grid properly) $U = \int dU = \int u dV$. Values are the log (base 10) of that, in the slightly odd units of gigajoules per radian. A factor of 2π wouldn't change anything, of course, but it seems inappropriate to integrate all the way around the sphere when Pc4s are longitudinally localized (a fact which was an important part of justifying a 2.5D approach).

Poloidal (Blue) and Toroidal (Red) Energy: 22mHz Current

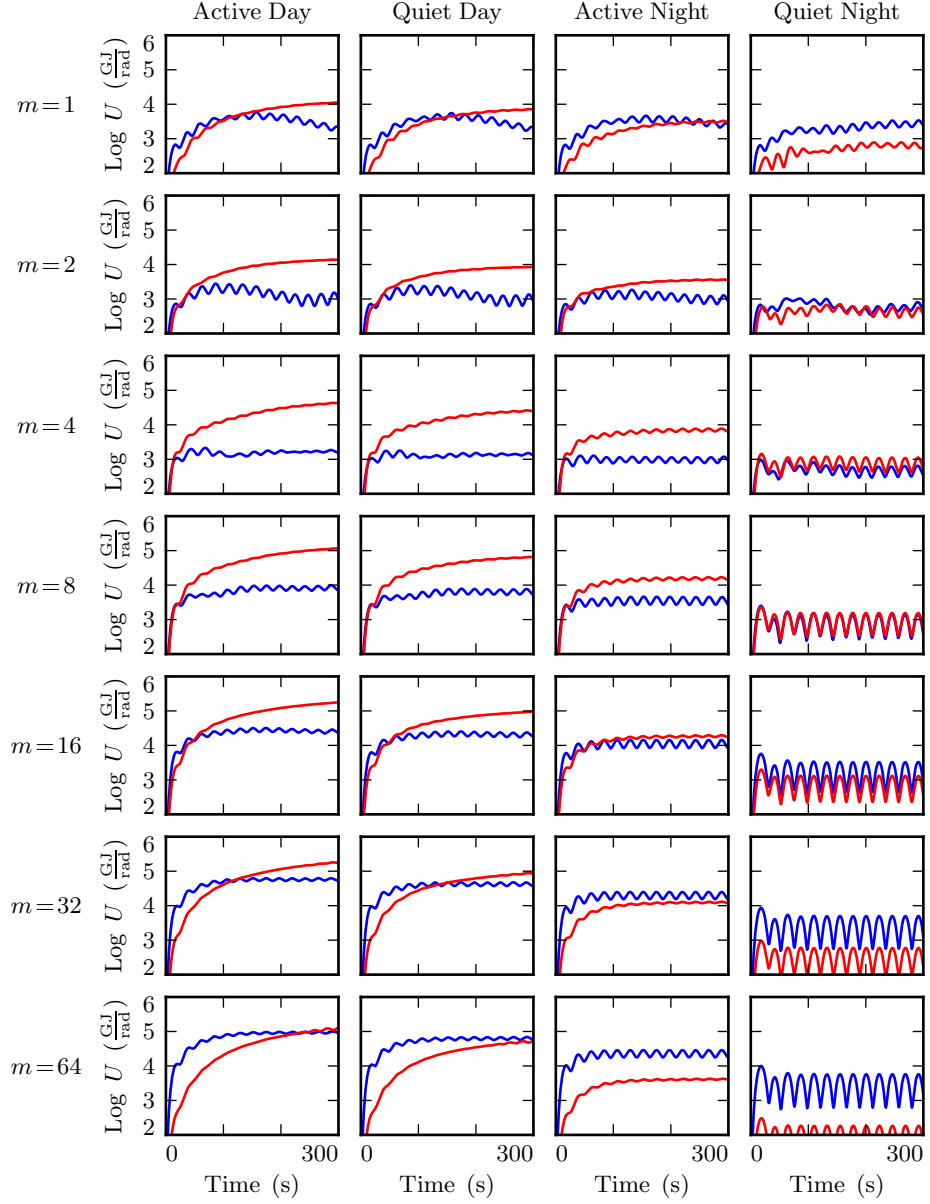


Figure 7.1: Driving is applied to the poloidal electric field. Over time, the energy rotates from the poloidal mode to the toroidal. The rotation time is affected by the azimuthal modenumber. Ionospheric conductivity also plays an important role.

In Figure 7.1, the rotation of energy from the poloidal mode to the toroidal mode is clear. Driving is strictly poloidal, yet the toroidal mode accumulates energy over time, and doesn't appear to give it back. The rotation happens faster for low- m simulations, qualitatively consistent with Mann's result; the time at which poloidal and toroidal energies are equal seems to even be linear in m , as he predicted (for well-behaved runs, at least).

At least, that's the case on the dayside, where the ionosphere is highly conducting.

On the nightside, the same isn't true in any meaningful way. Dissipation seems to outstrip rotation. Energy does not accumulate over numerous driving periods, as would be expected in resonance; it follows the driving up and down, as a damped-driven oscillator.

There is evidence that the rotation is still trying to happen. At low m , energy is distributed between the poloidal and toroidal mode before dissipating; at high m , the energy dissipates straight out of the poloidal mode, never having had a chance to rotate.

7.2 Resonant Shells

Looking a bit deeper, it's possible to comment on the structure of the poloidal and toroidal modes, not just their magnitudes.

(The following commentary applies to the dayside; on the nightside, there's never much by the way of resonance.)

In Figures 7.2 to 7.5, electromagnetic energy is binned by field line, averaged over volume (again, with respect to the Jacobian), and plotted as contours. All plots share a color scale.

The poloidal mode and the toroidal mode exhibit qualitatively different behavior, related to the fact that energy rotates from poloidal to toroidal, and not back.

At low m , energy rotates out of the poloidal mode so quickly that no resonance can form.

At high m , the Alfvén wave is guided. If the driving frequency lines up with the resonant frequency where it's delivered, the poloidal mode resonates strongly. Otherwise, again, no energy accumulates.

In no case does the poloidal mode demonstrate the ability to move energy across magnetic field lines.

On the other hand, the toroidal mode does resonate, even if the driving isn't resonant (though in that case the response is of course stronger). The toroidal mode transports energy across field lines until it encounters resonance, then accumulates energy there. Often, resonances are seen in multiple locations due to the non-monotonic Alfvén bounce frequency (recall Figure 3.4) as a function of L .

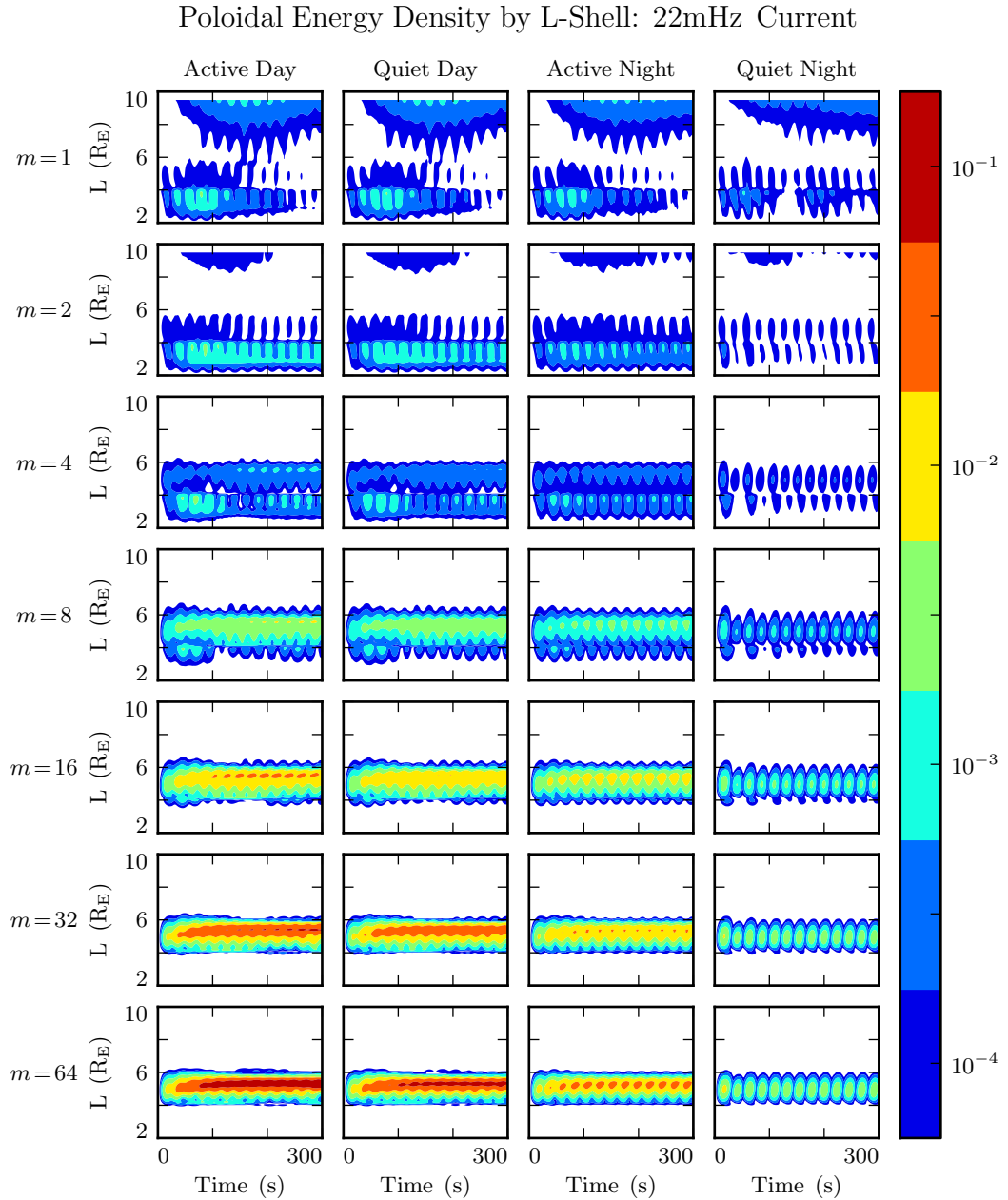


Figure 7.2: If m is small, energy rotates to the toroidal mode too fast to form a poloidal resonance. If m is large, the Alfvén wave is guided, so it resonates only if the driving frequency lines up with the resonant frequency where it's applied. The result is just one big – or perhaps even giant – pulsation.

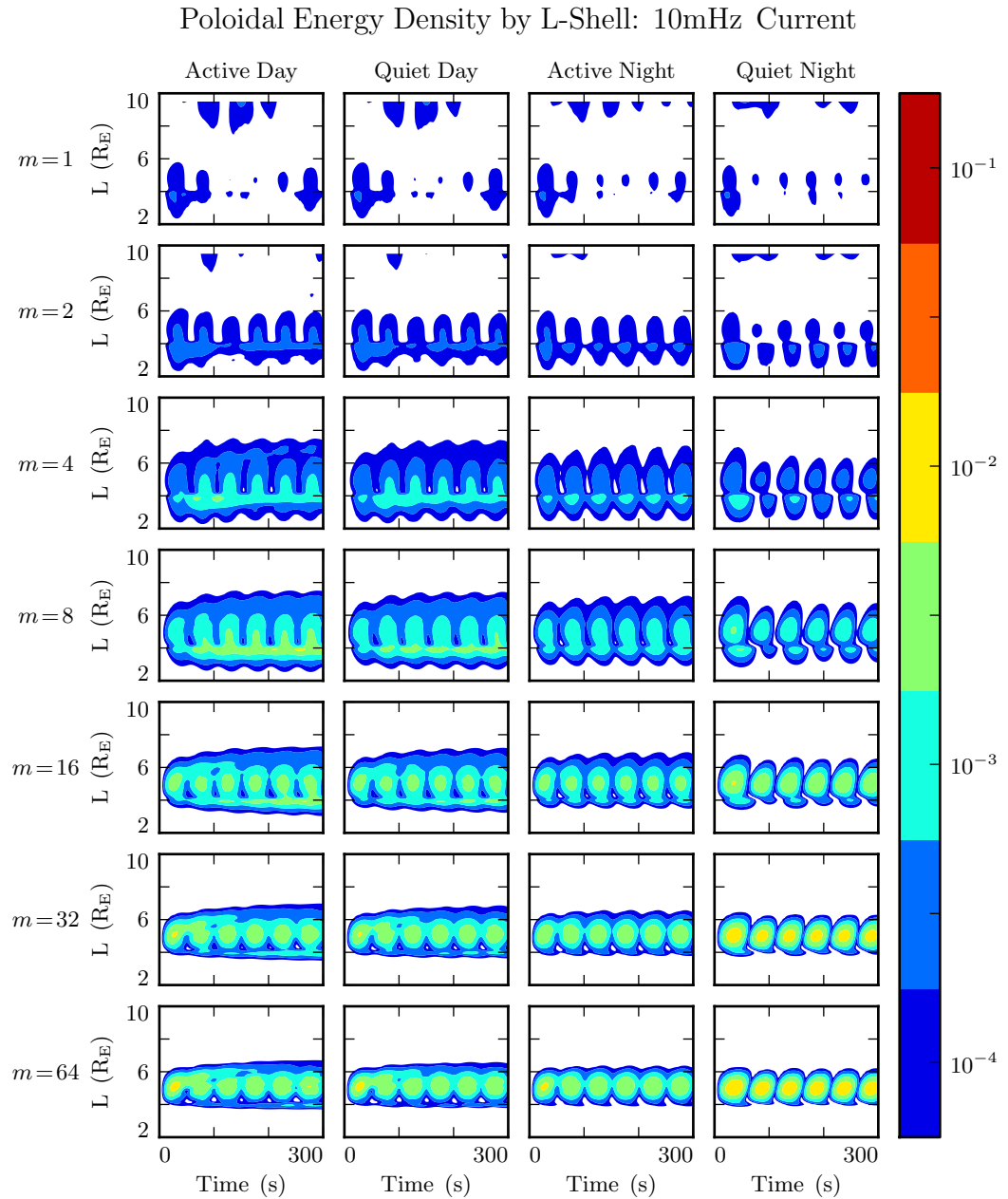


Figure 7.3: When the driving frequency doesn't line up with the location where it's delivered, there's basically no response. There is no movement of energy to a resonant field line, so no energy can accumulate over the course of multiple rounds of driving.

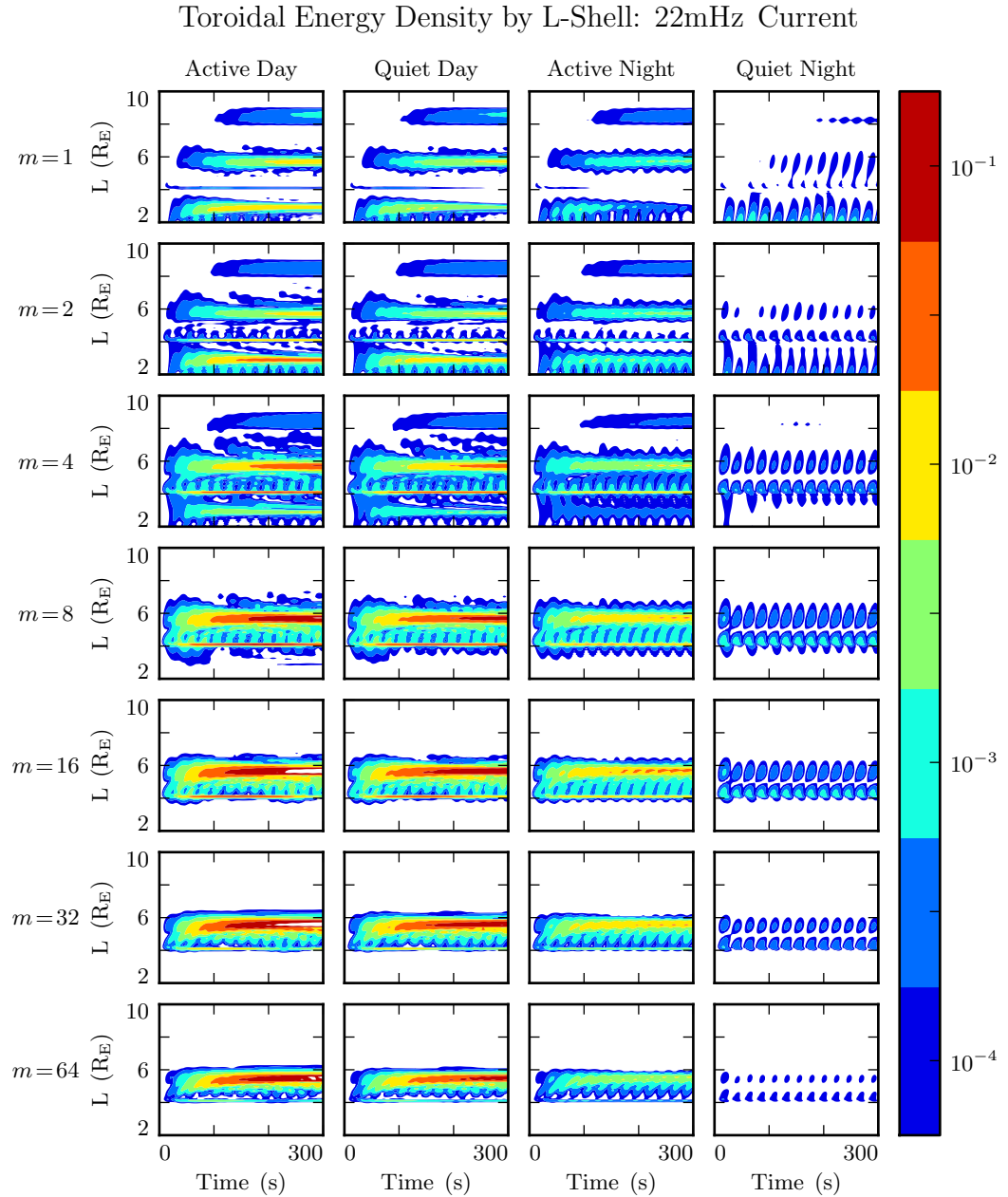


Figure 7.4: If the driving lines up with a nearby field line, the toroidal mode goes crazy! Resonance inside the plasmasphere. Resonance at the plasmapause. Resonance at the driving location. And (weak) attempt at a higher harmonic further out.

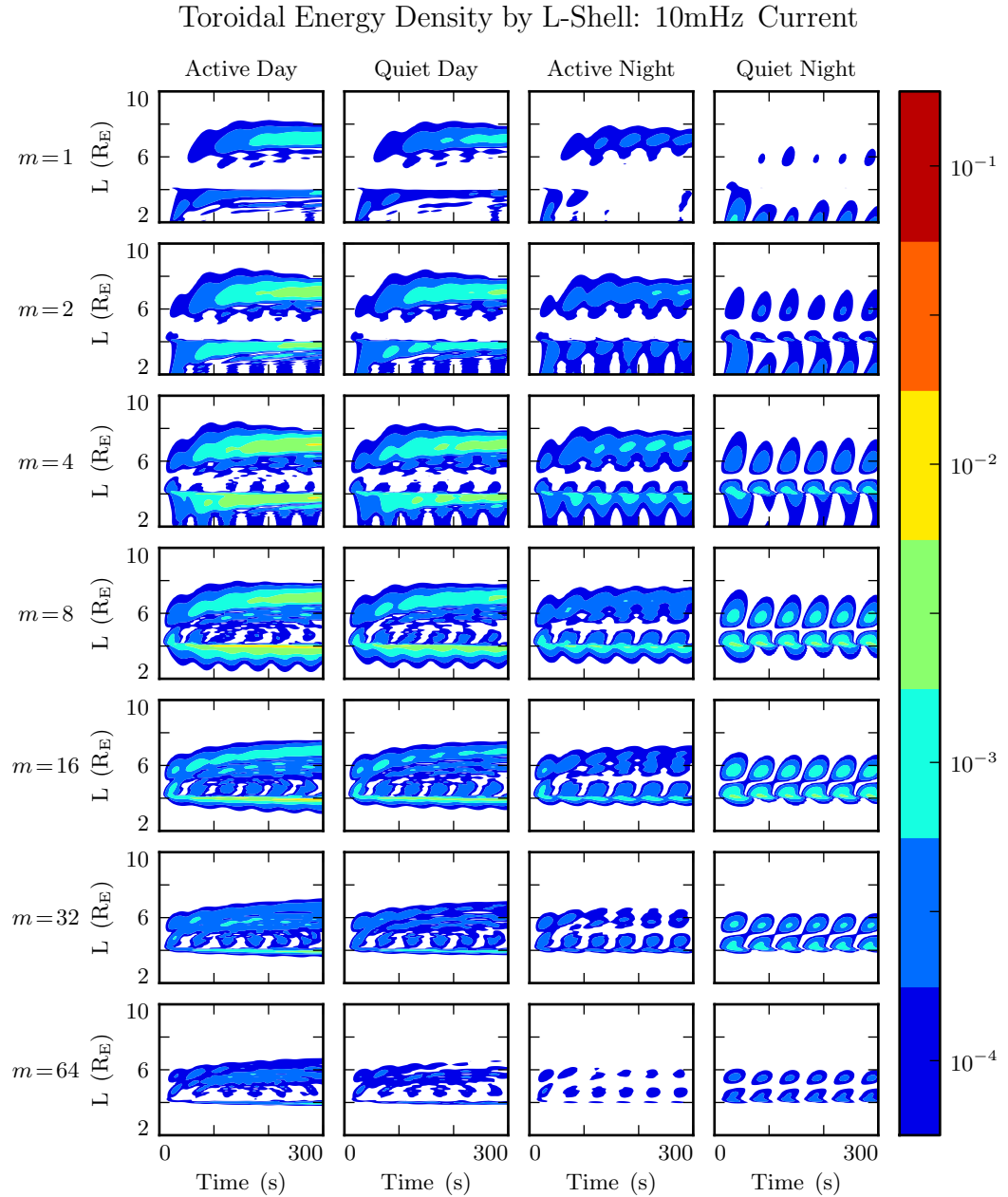


Figure 7.5: Even when not driven resonantly, the toroidal mode still makes the best of its situation. It steals what energy it can from the poloidal mode, carries it to the resonant L -shell, and gets to work. (In contrast, recall from Figure 7.3, in this situation the poloidal mode just does not accumulate energy.)

7.3 Significance for Giant Pulsations

Giant pulsations are (probably[32]) fundamental mode poloidal $Pc4$ pulsations with frequencies around 10 mHz and azimuthal modenumber around 20. They are large, and can sometimes be observed on the ground.

While this model makes no particular distinction between a giant pulsation and any other $Pc4$, the above results do line up with giant pulsation observations.

Giant pulsations aren't seen at small m . As shown in Section 7.1, low- m poloidal modes rotate to the toroidal mode too quickly to resonate effectively, even in the case of continuous driving at a locally-resonant frequency. The sweet spot seems to be around $m = 20$, more or less the same point where resonance becomes visible in Figure 7.2. Admittedly, giant pulsations are typically closer to 10 mHz than 22 mHz. It seems likely that qualitatively similar results would be encountered if the driving were moved to an L -shell with a bounce time of 10 mHz.

(Giant pulsations are seen at very large m , though not on the ground[4], due to damping by the ionosphere.)

TODO: Show some ground signatures. They get weak as m gets large.

Giant pulsations are monochromatic, and can be accompanied by “multiharmonic toroidal waves”[32]. Per Section 7.2, this is about what would be expected from a mishmash of poloidal driving. Poloidal modes of all frequencies rotate into the toroidal mode; resonant poloidal modes resonate; non-resonant poloidal modes become evanescent.

Giant pulsations often drift azimuthally. This model can't resolve azimuthal drift directly, of course, but can fake it by looking at complex phase. There has been some indication (not shown) of complex phase rotation in ground magnetic fields. However, at the boundary, it's difficult to disentangle which values are imaginary to indicate an azimuthal offset, and which are imaginary because of Hall coupling. Investigation is ongoing.

7.4 Electromagnetic Energy Gap

TODO: A preliminary search (and asking Bob) has not turned up anyone looking at this before, so it's hard to provide context.

Above, we considered the decay of energy from the poloidal mode to the toroidal mode. A natural follow up is, are there any other surprising trends in the distribution of energy?

As it turns out, yes!

In cases where the driving frequency does not line up with the local bounce frequency, energy doesn't accumulate particularly well in either the poloidal or the toroidal mode. Like a damped-driven oscillator, the system's behavior follows the input.

At low m , what energy there is divides itself more-or-less equally between the electric and magnetic fields.

As m increases, oddly, a gap appears. When the conductivity is high, the magnetic field holds more energy than the electric field. The disparity can be up to a factor of ~ 3 ; that is, 75 % of the energy in the magnetic field, and 25 % in the electric field. When conductivity is low, the opposite happens: energy concentrates in the electric field.

This lines up somewhat with what might be expected. When conductivity is low, it takes a larger electric field to induce the same current, and thus the same magnetic field. But it's not clear why this disparity only appears at large m , or why it does not appear when the driving is resonant.

Maybe it's a timing issue? A relationship between the bounce time (which is more or less independent of m) and the rotation time (which depends on m).

TODO: How is the compressional magnetic field brought into these calculations? It exists only at small m . It's never particularly large, it also gets added to the zeroth-order field before squaring.

Electric (Blue) and Magnetic (Red) Energy: 10mHz Current

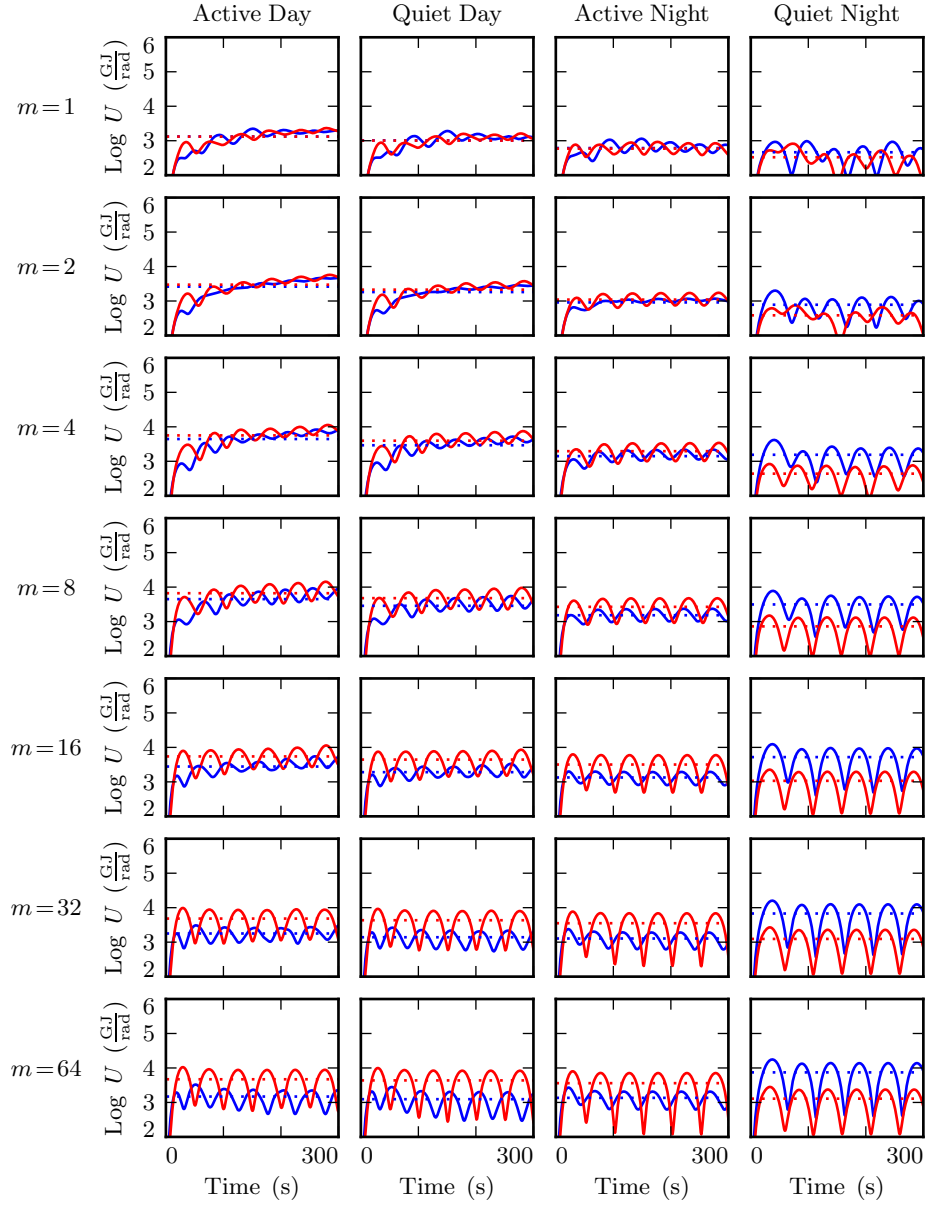


Figure 7.6: In the absence of resonant driving, a disparity emerges at large m between the energy in the magnetic field and the energy in the electric field. The sign of the difference depends on the ionospheric conductivity.

Electric (Blue) and Magnetic (Red) Energy: 22mHz Current

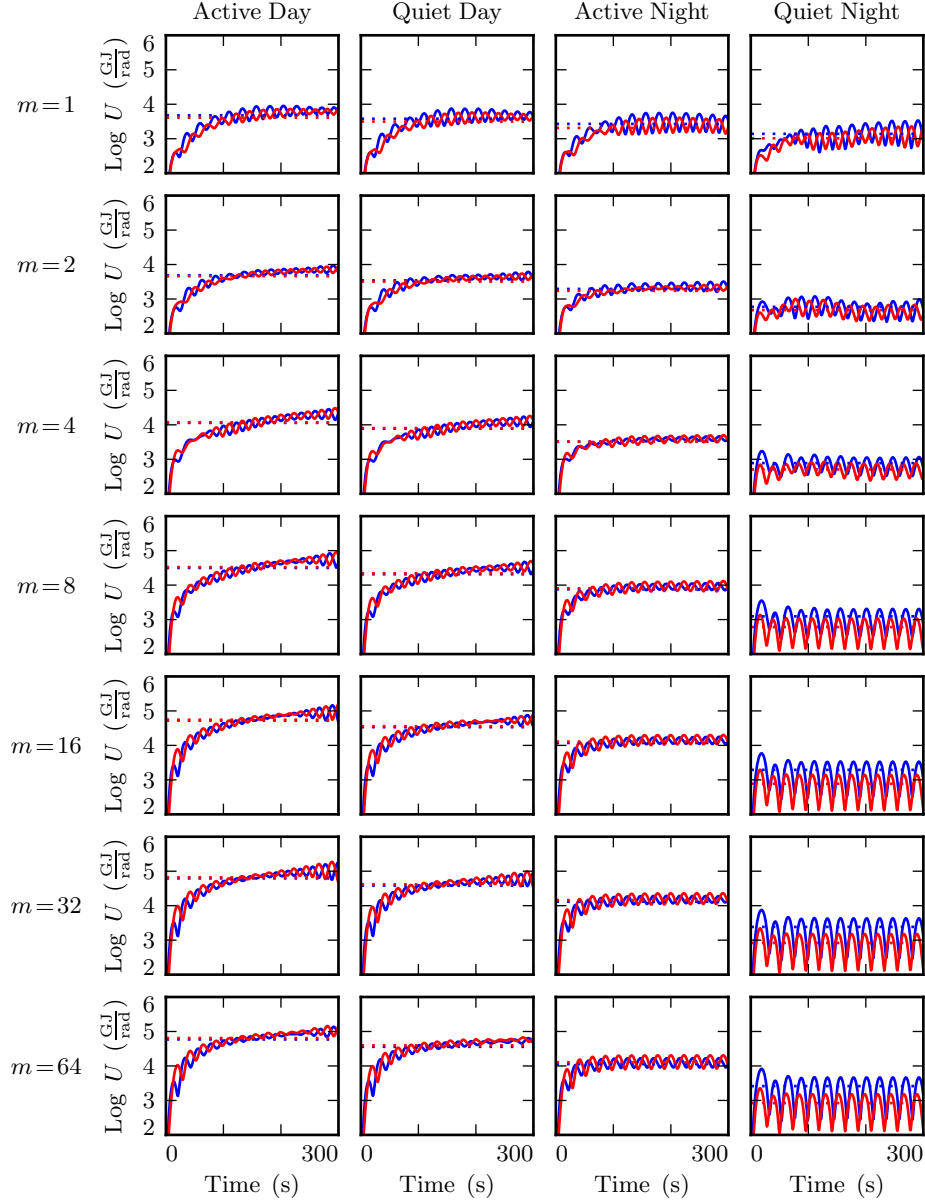


Figure 7.7: When driving is resonant, energy is distributed almost exactly half-and-half between the electric and magnetic fields, regardless of m . The rightmost profile still shows a gap, likely because the ionospheric conductivity in that model is low enough that nothing ever resonates.

Chapter 8

Conclusion

8.1 Summary of Results

TODO: Write this.

8.2 Future Work

Arbitrary deformation of grid. Get $\hat{e}_i = \frac{\partial}{\partial u^i} \underline{x}$, then $g_{ij} = \hat{e}_i \cdot \hat{e}_j$, then invert the metric tensor for contravariant components.

MPI. Some benchmarks with time to compute vs time to broadcast. At what problem scale does additional parallelization make sense?

Driving based on events? Wouldn't be that hard.

Test particles? Seems silly. Watching something drift-bounce resonate will require making assumptions about what's going on on the other face of the planet.

References

- [1] W. J. Hughes. Magnetospheric ulf waves: A tutorial with a historical perspective. In M. J. Engebretson, K. Takahashi, and M. Scholer, editors, *Solar Wind Sources of Magnetospheric Ultra-Low-Frequency Waves*, volume 81 of *Geophys. Monogr.*, pages 1–12. American Geophysical Union, Washington, DC, 1994.
- [2] J. W. Dungey. The attenuation of alfvén waves. *J. Geophys. Res.*, 59(3):323–328, 1954.
- [3] W. J. Hughes and D. J. Southwood. The screening of micropulsation signals by the atmosphere and ionosphere. *J. Geophys. Res.*, 81(19):3234–3240, 1976.
- [4] Kazue Takahashi, Michael D. Hartinger, Vassilis Angelopoulos, Karl-Heinz Glassmeier, and Howard J. Singer. Multispacecraft observations of fundamental poloidal waves without ground magnetic signatures. *J. Geophys. Res. Space Physics*, 118:4319–4334, 2013.
- [5] Lei Dai, Kazue Takahashi, Robert Lysak, Chi Wang, John R. Wygant, Craig Kletzing, John Bonnell, Cynthia A. Cattell, Charles W. Smith, Robert J. MacDowall, Scott Thaller, Aaron Breneman, Xiangwei Tang, Xin Tao, and Lunjin Chen. Storm time occurrence and spatial distribution of pc4 poloidal ulf waves in the inner magnetosphere: A van allen probes statistical study. *J. Geophys. Res. Space Physics*, 120:47484762, 2015.
- [6] M. J. Engebretson, L. J. Zanetti, T. A. Potemra, W. Baumjohann, H. Lühr, and M. H. Acuna. Simultaneous observation of pc 34 pulsations in the solar wind and

in the earth's magnetosphere. *J. Geophys. Res. Space Physics*, 92:10053–10062, 1987.

- [7] A. N. Jaynes, M. R. Lessard, K. Takahashi, A. F. Ali, D. M. Malaspina, R. G. Michell, E. L. Spanswick, D. N. Baker, J. B. Blake, C. Cully, E. F. Donovan, C. A. Kletzing, G. D. Reeves, M. Samara, H. E. Spence, and J. R. Wygant. Correlated pc45 ulf waves, whistler-mode chorus, and pulsating aurora observed by the van allen probes and ground-based systems. *J. Geophys. Res. Space Physics*, 120:87498761, 2015.
- [8] D. J. Southwood. A general approach to low-frequency instability in the ring current plasma. *J. Geophys. Res.*, 81(19):3340–3348, 1976.
- [9] W. J. Hughes. The effect of the atmosphere and ionosphere on long period magnetospheric micropulsations. *Planet. Space Sci.*, 22:1157–1172, 1974.
- [10] Carl Greifinger and Phyllis S. Greifinger. Theory of hydromagnetic propagation in the ionospheric waveguide. *J. Geophys. Res.*, 73(23):7473–7490, 1968.
- [11] Shigeru Fujita and Tsutomu Tamao. Duct propagation of hydromagnetic waves in the upper ionosphere, 1, electromagnetic field disturbances in high latitudes associated with localized incidence of a shear alfvén wave. *J. Geophys. Res.*, 93(A12):14665, 1988.
- [12] Henry R. Radoski. A theory of latitude dependent geomagnetic micropulsations: The asymptotic fields. *J. Geophys. Res.*, 79, 1974.
- [13] Ian R. Mann and Andrew N. Wright. Finite lifetimes of ideal poloidal alfvén waves. *J. Geophys. Res.*, 100:23677–23686, 1995.
- [14] Ian R. Mann, Andrew N. Wright, and Alan W. Hood. Multiple-timescales analysis of ideal poloidal alfvén waves. *J. Geophys. Res.*, 102(A2):2381–2390, 1997.
- [15] Robert L. Lysak, Colin L. Waters, and Murray D. Sciffer. Modeling of the ionospheric alfvén resonator in dipolar geometry. *J. Geophys. Res. Space Physics*, 118, 2013.

- [16] R. L. Lysak and A. Yoshikawa. Resonant cavities and waveguides in the ionosphere and atmosphere. In K. Takahashi, P. J. Chi, R. E. Denton, and R. L. Lysak, editors, *Magentospheric ULF Waves: Synthesis and New Directions*, volume 169 of *Geophys. Monogr.*, page 289. American Geophysical Union, Washington, DC, 2006.
- [17] C. L. Waters, R. L. Lysak, and M. D. Sciffer. On the coupling of fast and shear alfvén wave modes by the ionospheric hall conductance. *Earth Planets Space*, 65:385–396, 2013.
- [18] Robert L. Lysak. Magnetosphere-ionosphere coupling by alfvén waves at midlatitudes. *J. Geophys. Res.*, 109, 2004.
- [19] J. R. Woodroffe and R. L. Lysak. Ultra-low frequency wave coupling in the ionospheric alfvén resonator: Characteristics and implications for the interpretation of ground magnetic fields. *J. Geophys. Res.*, 117:A03223, 2012.
- [20] Henry R. Radoski. A note on oscillating field lines. *J. Geophys. Res.*, 72(1), 1967.
- [21] Jeffrey A. Proehl, William Lotko, Igor Kouznetsov, and Shireen D. Geimer. Ultralow-frequency magnetohydrodynamics in boundary-constrained geomagnetic flux coordinates. *J. Geophys. Res.*, 107(A9):1225, 2002.
- [22] W. D. D'haeseleer, W. N. G. Hitchon J. D. Callen, and J. L. Shohet. *Flux Coordinates and Magnetic Field Structure*. Springer-Verlag, New York, 1991.
- [23] A. Einstein. Die grundlage der allgemeinen relativitätstheorie. *Ann. Phys.*, 354:769–822, 1916.
- [24] Michael C. Kelley. *The Earth's Ionosphere*. Academic Press, San Diego, second edition, 1989.
- [25] Brian C. Hall. *Lie Groups, Lie Algebras, and Representations*. Graduate Texts in Mathematics. Springer, New York, second edition, 2015.
- [26] NASA. Coordinated data analysis (workshop) web.
- [27] Robert L. Lysak and Yan Song. Development of parallel electric fields at the plasma sheet boundary layer. *J. Geophys. Res. Space Physics*, 116, 2011.

- [28] Jay P. Boris. A physically motivated solution of the alfvén problem. *NRL Memorandum Report*, 2167, 1970.
- [29] Robert L. Lysak and Yan Song. A three-dimensional model of the propagation of alfvén waves through the auroral ionosphere: first results. *Adv. Space Res.*, 28:813–822, 2001.
- [30] Kjell Rönnmark and Maria Hamrin. Auroral electron acceleration by alfvén waves and electrostatic fields. *J. Geophys. Res.*, 105:25333–25344, 2000.
- [31] D. Q. Ding, R. E. Denton, M. K. Hudson, and R. L. Lysak. An mhd simulation study of the poloidal mode field line resonance in the earth’s dipole magnetosphere. *J. Geophys. Res.*, 100:63–77, 1995.
- [32] Kazue Takahashi, Karl-Heinz Glassmeier, Vassilis Angelopoulos, John Bonnell, Yukitoshi Nishimura, Howard J. Singer, and Christopher T. Russell. Multisatellite observations of a giant pulsation event. *J. Geophys. Res.*, 116:A11223, 2011.

Appendix A

Differential Geometry

TODO: Not sure that a glossary or list of acronyms will be necessary, but here are the examples from the template.

A.1 Glossary

- **Cosmic-Ray Muon (CR μ)** – A muon coming from the abundant energetic particles originating outside of the Earth's atmosphere.

A.2 Acronyms

Table A.1: Acronyms

Acronym	Meaning
CR μ	Cosmic-Ray Muon